Cosmological and High Energy Physics implications from gravitational-wave background searches in LIGO-Virgo-KAGRA's O1-O4a runs

The LIGO Scientific Collaboration, The Virgo Collaboration, and The KAGRA Collaboration*

(Dated: November 3, 2025)

We search for gravitational-wave background signals produced by various early Universe processes in the Advanced LIGO O4a dataset, combined with the data from the earlier O1, O2, and O3 (LIGO-Virgo) runs. The absence of detectable signals enables powerful constraints on fundamental physics. We derive gravitational-wave background energy density upper limits from the O1-O4a data to constrain parameters associated with various possible processes in the early Universe: first-order phase transitions, cosmic strings, domain walls, stiff equation of state, axion inflation, second-order scalar perturbations, primordial black hole binaries, and parity violation. In our analyses, the presence of an astrophysical background produced by compact (black hole and neutron star) binary coalescences throughout the Universe is also considered. We address the implications for various cosmological and high energy physics models based on the obtained parameter constraints. We conclude that LIGO-Virgo data already yield significant constraints on numerous early Universe scenarios.

I. INTRODUCTION

Advanced LIGO [1], Advanced Virgo [2] and KAGRA [3] have completed three observational runs. LIGO, Virgo and KAGRA are now in their fourth observational run, O4, which began in May 2023. The O4a part of the run started on May 24, 2023, going until Jan. 16th, 2024 [4]. Data acquired in these observation runs have resulted in a series of novel scientific pursuits. This includes discovery of over 200 compact binary (black hole and neutron star) mergers [5], increasingly stringent tests of General Relativity [6], multi-messenger measurements of the Hubble constant [7], and measurements of the neutron star equation-of-state [8].

One of the primary targets of these observations is the gravitational-wave background produced by a superposition of a large number of uncorrelated gravitational-wave signals [9]. Observations of stellar mass compact binary mergers by Advanced LIGO and Advanced Virgo imply that a gravitational-wave background of astrophysical origin [10–15] should exist and that it may be detectable by the LIGO-Virgo-KAGRA network in the near future [16–19]. Furthermore, a gravitational-wave background could be of cosmological origin, generated in a variety of processes in early phases of the Universe. Consequently, gravitational-wave background searches can be used to probe high energy physics models at energy scales beyond the ones reached at the Large Hadron Collider [20], and to explore early Universe cosmological scenarios [21–24].

In what follows, we present searches for a gravitational-wave background produced by various cosmological models, using the LIGO O1 [25], O2, O3 [26] and O4a [27, 28] data, plus Virgo O3 [29] data, and we report the resulting constraints on their parameters. Motivations for considering sources of a cosmological gravitational-wave background descend from open questions of fundamental physics. Indeed, despite the extraordinary success of the Standard Model of Particle Physics and Cosmology, our understanding of basic aspects of fundamental physics is still incomplete. The nature of dark matter, the origin of the matter/anti-matter asymmetry, the explanation of the neutrino masses, and the realization of inflation remain as important open questions. In order to solve these issues, scenarios of physics beyond the Standard Model are investigated and are under scrutiny in astro-particle experiments, from colliders to telescopes. Many of these beyond the Standard Model scenarios also imply novel phenomena happening in the very early stages of the Universe, potentially leaving footprints in the form of a gravitational-wave background. The models for which we conduct gravitational-wave background searches are first-order phase transitions, cosmic strings, domain walls, stiff equation of state, axion inflation, second-order scalar perturbations, primordial black holes, and parity violation.

The first three models (first-order phase transitions, cosmic strings, domain walls) we consider are related to cosmological phase transitions, common in theories with spontaneously broken symmetries [30–32]. If the phase transition is first-order, it can generate a gravitational-wave background [33]. Phase transitions followed by spontaneously broken symmetries can lead to topological defects, such as cosmic strings [34, 35] and domain walls [36–42], extended objects in the Universe that can produce a gravitational-wave background.

The next three models (stiff equation of state, axion inflation, second-order scalar perturbations) we study lead to a gravitational-wave background generated during inflation. While single-field slow-roll inflation within the ΛCDM cosmological model predicts a gravitational-wave background that is too weak to be observed with current detectors, other inflationary models may produce a detectable gravitational-wave background. For an exotic early Universe cosmological model with a stiff equation of state [43–51], we explore the gravitational-wave

* Full author list given at the end of the article.

background generated during inflation [50–53]. For the axion inflation model, we consider a coupling between the scalar field driving inflation and an SU(2) gauge field, and calculate the produced gravitational-wave background [54–57]. For second-order scalar perturbations [58], we estimate the gravitational-wave background induced by primordial curvature perturbations [59–63].

Next we study a gravitational-wave background generated by mergers of primordial black holes [64] that could have formed by a variety of mechanisms in the early Universe. Finally, we study a gravitational-wave background that exhibits chiral polarization. We consider a model-independent parametrization of such a background, as well as a particular case where parity violation originates from axion inflation [65].

For each of these cosmological models, the absence of a gravitational-wave background constrains their parameters. The results of our analysis show that the LIGO-Virgo O1-O4a data can already be used to successfully derive new constraints on a wide range of theories beyond the Standard Model.

Formalism and methodology: The gravitational-wave background is quantified in terms of its energy density per logarithmic frequency interval, and compared to the critical energy density of the Universe. Specifically,

$$\Omega_{\rm GW}(f) = \frac{f}{\rho_c}\frac{{\rm d}\rho_{\rm GW}}{{\rm d}f} \ , \tag{1}$$

where $\rho_{\rm GW}$ is the energy density of gravitational waves, the critical energy density of the Universe is $\rho_c = 3c^2H_0^2/(8\pi G) \approx 7.7\times10^{-9}$ erg cm^{-3}, $H_0 = 100\ h$ km/s/Mpc is the Hubble constant with $h = 0.68$ from the Planck measurements [66], c the speed of light, and G Newton's constant. The gravitational-wave background spectrum is often approximated by the power-law (PL) form with the spectral index α

$$\Omega^{\rm PL}_{\rm GW}(f) = \Omega_{\rm ref}\left(\frac{f}{f_{\rm ref}}\right)^{\alpha} \ , \tag{2}$$

where $\Omega_{\rm ref}$ is the gravitational-wave energy density at the reference frequency $f_{\rm ref}$. A background produced by compact binary mergers from population I or II stars can be approximated as having $\alpha = 2/3$ [67]. Cosmological backgrounds can also be typically approximated as power laws, or as broken power laws, as we show in the following.

For the first three observing runs, the LIGO-Virgo-KAGRA collaboration reported an upper limit on the strength of an isotropic gravitational-wave background of $\Omega_{\rm GW} \leq 5.8\times10^{-9}$ for $\alpha = 0$ and 95% credible level [68] with 99% of the sensitivity coming from the band (20–76.6) Hz. For $\alpha = 2/3$, the limit was $\Omega_{\rm GW}(25{\rm Hz}) \leq 3.4\times10^{-9}$ in the band (20–90.6) Hz. This upper bound was derived from the LIGO data acquired during O1, O2, and O3 observing runs, as well as Virgo data of O3. There have also been searches for backgrounds with non-standard polarizations, such as scalar and vector (in addition to tensor) [69, 70]. Anisotropic backgrounds have been also explored [15, 71].

The O4a data, combined with the data from O1, O2 and O3, do not provide evidence for the detection of a gravitational-wave background [19]. As such, an upper limit of $\Omega_{\rm GW} \leq 2.8\times10^{-9}$ is set for $\alpha = 0$ and 95% confidence, with 99% of the sensitivity coming from the band (20 – 58.2) Hz. For $\alpha = 2/3$ the limit is $\Omega_{\rm GW}(25{\rm Hz}) \leq 2.0\times10^{-9}$ in the band (20 – 86.8) Hz [19]. The LIGO-Virgo-KAGRA Collaboration has also searched for an anisotropic gravitational-wave background [71].

To derive constraints on the cosmological model parameters, we perform a Bayesian analysis [72] using the data from the LIGO-Virgo O1-O4a observing runs, following the methods developed in [73]. Assuming the cross correlation estimator $\hat{C}_{IJ}(f)$ [68] is Gaussian-distributed, we write the following likelihood function

$$p(\hat{C}_{IJ}(f)|\boldsymbol{\theta},\lambda) \propto \exp\left[-\frac{1}{2}\sum_f \frac{[\hat{C}_{IJ}(f) - \lambda\,\Omega_{\rm GW}(f,\boldsymbol{\theta})]^2}{\sigma^2_{IJ}(f)}\right], \tag{3}$$

using data from detectors I and J, while $\sigma^2_{IJ}(f)$ is the variance. Both $\hat{C}_{IJ}(f)$ and $\sigma^2_{IJ}(f)$ are data products from the LIGO-Virgo-KAGRA collaboration isotropic gravitational-wave background search analysis [19], where they are calculated from the LIGO-Virgo data. It is assumed that such an isotropic search does not have correlated noise between detectors I and J, for example, from correlated magnetic noise [74]. Hence a standard Gaussian noise model is preferred [68], and the potential contribution from correlated magnetic noise (Schumann resonances) [75] can be neglected [19]. The function $\Omega_{\rm GW}(f,\boldsymbol{\theta})$ corresponds to the model considered, described by the set of parameters $\boldsymbol{\theta}$, while the parameter λ, which we marginalize over, accounts for the detectors' calibration uncertainties [19]. A minimum of two detectors are needed in order to conduct this analysis. The two LIGO detectors contribute the most to the correlation due to the smallest distance separation in the network, their optimal alignment [76, 77], and their sensitivities [68].

In our analyses, we take into account the contribution from an isotropic astrophysical background of compact binary coalescences (CBC) $\Omega_{\rm CBC}(f,\boldsymbol{\theta}_{\rm CBC}) = \Omega_{\rm CBC}(f,\Omega_{\rm ref},\alpha)$, which we model by Eq. 2 where $f_{\rm ref} = 25$ Hz [68]. The cosmologically produced gravitational-wave background is $\Omega_{\rm Cosmo}(f,\boldsymbol{\theta}_{\rm Cosmo})$. The total gravitational-wave background is

$$\Omega_{\rm GW}(f,\boldsymbol{\theta}) = \Omega_{\rm CBC}(f,\Omega_{\rm ref},\alpha) + \Omega_{\rm Cosmo}(f,\boldsymbol{\theta}_{\rm Cosmo}). \tag{4}$$

This publication is organized as follows: we present limits on various cosmological models in the following sections; first-order phase transitions in Sec. II; cosmic strings in Sec. III; domain walls in Sec. IV; stiff equation of state in Sec. V; axion inflation in Sec. VI; second-order

scalar perturbations in Sec. VII; primordial black holes in Sec. VIII; and parity violation in Sec. IX. For each of the eight scenarios we discuss the motivation, we present the model considered, and give the constraints to the model parameters using O1-O4a LIGO-Virgo data. Conclusions are given in Sec. X.

II. FIRST-ORDER PHASE TRANSITIONS

A. Motivation

Cosmological phase transitions are among the most well-motivated early Universe phenomena we anticipate (see e.g. [30–32]). They are a common feature of particle physics models that exhibit symmetry breaking. The phase transition is first-order when the effective potential of the theory develops a new minimum (true vacuum) with a free energy density lower than that of the minimum at high temperature (false vacuum), and both are separated by a potential barrier. The Universe then violently transitions from the symmetric higher energy false vacuum to the broken lower energy true vacuum. A first order phase transition is a powerful source of a gravitational-wave background.

Given our knowledge of the cosmological history and particle physics, such transitions could have occurred within the first one-trillionth of a second after the Big Bang, at energies higher than those accessible in present-day particle accelerators. Their gravitational wave imprints would be an important key to determining the correct theory beyond the Standard Model realized in Nature.

The Standard Model itself undergoes two phase transitions: the electroweak phase transition due to the breaking of electroweak symmetry, and the confinement-deconfinement phase transition due to chiral symmetry breaking in quantum chromodynamics (QCD). Neither of these Standard Model phase transitions is first order (or generates stable topological defects), thus no corresponding gravitational wave signatures are expected.

However, many extensions of the Standard Model with enlarged symmetry structures at high energies necessarily undergo spontaneous symmetry breaking (for sufficiently high reheating temperature). Such a first order phase transition corresponds to nucleation of bubbles of true vacuum in various points in the Universe. Those bubbles then expand, collide with each other, and eventually fill out the entire space. During this process, gravitational waves are generated from processes such as bubble collisions [78, 79], sound waves propagating in the early Universe plasma [80, 81], and magnetohydrodynamic turbulence [82], with the first two contributions being typically dominant (see e.g. [33] and references therein).

The strong connection of the resulting primordial gravitational wave background to particle physics provides gravitational wave astronomy with a unique opportunity to probe regions of parameter space of physics models completely inaccessible in any other types of experiments. This includes various extensions of the Standard Model, e.g., models with an extended electroweak gauge sector [83–85], theories with dark sectors [86–88], axion models [89–91], unification models [92, 93], supersymmetric theories [94–96], or theories with extra dimensions [97]. In turn, the information about physics at energies beyond the electroweak scale may provide insight into solutions to problems such as the nature of dark matter or the origin of the matter-antimatter asymmetry of the Universe.

As it has recently been shown based on the LIGO-Virgo observing runs O1-O3, already current data can be used to provide meaningful constraints on the parameters of first order phase transitions [98]. This method was successfully applied to particle physics models in the context of supercooled transitions (see e.g. [99, 100]), leading to novel constraints on beyond-Standard Model theories [101]. In the following, we utilize the LIGO-Virgo O1-O4a data to derive new and improved bounds on the parameters of early Universe first order phase transitions.

B. Model

In this scenario the cosmological component $\Omega_{\rm Cosmo}$ of the gravitational wave background in Eq. (4) depends on the parameters describing the phase transition, i.e. on the details of the particle physics model. From an effective theory point of view, a first order phase transition can be fully described by just several parameters: v_w – the bubble wall velocity (given in units of the speed of light), $T_{\rm PT}$ – the temperature of the phase transition, $\alpha_{\rm PT}$ – the strength of the phase transition, which is equal to the density of the energy released divided by the energy density of radiation, κ – the fraction of the energy corresponding to a given source, β – the inverse time duration of the transition, and g_* – the number of effective degrees of freedom (equal to 106.75 in the Standard Model at high temperatures).

In our analysis we first discuss the sound wave contribution which is typically dominant in case of thermal phase transitions (where friction from the Standard Model plasma is relevant), and then focus on the bubble collision contribution which is the leading source of gravitational waves for vacuum phase transitions (where friction is negligible). We disregard magnetohydrodynamic turbulence since its effects are typically subdominant and their characterization is subject of ongoing research. As for the gravitational wave background spectral shape for these two types of contributions, we select two representative forms, while acknowledging the fact that new results and simulations are continuously proposed in the literature (see discussion after Eq. (10)).

Sound wave contribution

We first address the leading source of gravitational waves for a thermal first order phase transition which

comes from sound waves in the primordial plasma, and is caused by the coupling between the scalar field undergoing the phase transition and the thermal bath [80, 81, 102]. A fruitful description of the physics of this process is provided by the sound shell model [103–105], although its accuracy has been challenged [102, 106]. The result of numerical simulations yields [81, 107]

$$h^2\Omega_{\rm SW}(f) \approx (1.86\times10^{-5})\, v_w \left(\frac{H_{\rm PT}}{\beta}\right)\left(\frac{\alpha_{\rm PT}\,\kappa_{\rm sw}}{\alpha_{\rm PT}+1}\right)^2\left(\frac{100}{g_*}\right)^{\frac{1}{3}} \times \frac{(f/f_{\rm sw})^3}{\left[1+0.75\,(f/f_{\rm sw})^2\right]^{\frac{7}{2}}}\,\Upsilon\,, \quad (5)$$

where the peak frequency $f_{\rm SW}$ is

$$f_{\rm SW} = \frac{(1.9\times10^{-5}\ {\rm Hz})}{v_w}\left(\frac{\beta}{H_{\rm PT}}\right)\left(\frac{T_{\rm PT}}{100\ {\rm GeV}}\right)\left(\frac{g_*}{100}\right)^{\frac{1}{6}}, \quad (6)$$

$H_{\rm PT}$ is the Hubble constant at the phase transition, $\kappa_{\rm sw}$ is the fraction of the latent heat transformed into the bulk motion of the plasma [108]

$$\kappa_{\rm SW} = \frac{\alpha_{\rm PT}}{0.73+0.083\sqrt{\alpha_{\rm PT}}+\alpha_{\rm PT}}\,, \quad (7)$$

and the suppression factor Υ due to the finite lifetime of sound waves is [105, 109]

$$\Upsilon = 1-\frac{1}{\left(1+8\pi^{1/3}v_w\left(\frac{H_{\rm PT}}{\beta}\right)\left(\frac{\alpha_{\rm PT}+1}{3\alpha_{\rm PT}\kappa_{\rm SW}}\right)^{1/2}\right)^{1/2}}\,, \quad (8)$$

derived assuming a lifetime on the order of the timescale for the onset of turbulence.

Bubble collision contribution

In some cases, e.g., when the first order phase transition occurs in the vacuum of a dark sector without sizable interactions with the Standard Model, the sound wave contribution is suppressed and the bubble collision part becomes dominant. The corresponding spectrum is obtained within the envelope approximation by assuming a zero width for the bubble wall and neglecting contributions from overlapping bubble segments [79, 110, 111]. It is given by [107, 112], using numerical simulations,

$$h^2\Omega_{\rm BC}(f) \approx \frac{(1.66\times10^{-5})\,v_w^3}{1+2.4v_w^2}\left(\frac{H_{\rm PT}}{\beta}\right)^2\left(\frac{\alpha_{\rm PT}\,\kappa_{\rm BC}}{\alpha_{\rm PT}+1}\right)^2 \times \left(\frac{100}{g_*}\right)^{\frac{1}{3}}\frac{(f/f_{\rm BC})^{2.8}}{1+2.8(f/f_{\rm BC})^{3.8}}\,, \quad (9)$$

where the peak frequency $f_{\rm BC}$ is

$$f_{\rm BC} = \frac{(10^{-5}\ {\rm Hz})}{1.8-0.1v_w+v_w^2}\left(\frac{\beta}{H_{\rm PT}}\right)\left(\frac{T_{\rm PT}}{100\ {\rm GeV}}\right)\left(\frac{g_*}{100}\right)^{\frac{1}{6}}, \quad (10)$$

and $\kappa_{\rm BC}$ is the fraction of the latent heat deposited into the bubble front [82]. We will take $\kappa_{\rm BC}=1$ for concreteness. The shape of the spectrum at low frequencies $\sim f^{2.8}$, close to the expected $\sim f^3$ from causality, whereas at high frequencies $\sim 1/f$ from the dominant single bubble contribution [112].

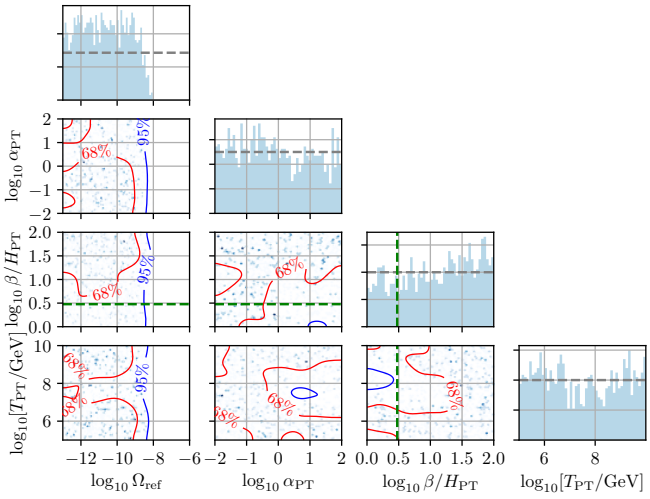

FIG. 1. Constraints from the LIGO-Virgo observing runs O1-O4a data on the first order phase transition parameters $\alpha_{\rm PT}$, $\beta/H_{\rm PT}$, and $T_{\rm PT}$, assuming a dominant sound wave contribution and taking into account the CBC background. The priors selected are shown in Table I. The 95% and 68% confidence level exclusion contours are shown in blue and red, respectively. Clearly, less conservative choices of priors could lead to stronger constraints. The green lines correspond to $\beta/H_{\rm PT}=(8\pi)^{1/3}$.

While we will use Eq. (9) in our analysis, we note that the precise shape of the gravitational-wave spectrum for bubble collisions is not fully settled. It was reported in [113] that simulations beyond the envelope approximation yield at high frequencies $\sim 1/f^{1.5}$. In [114] a dependence on wall thickness was found to change the high-frequency spectrum from $\sim 1/f^{1.4}$ to $\sim 1/f^{2.3}$ with increasing thickness. Further variations of the spectrum were discussed in [115–118]. In the next section we will comment on how our results change by considering varying power law indices.

C. Constraints using O1-O4a LIGO-Virgo data

Here we determine the 95% confidence level (CL) upper limits on the strength of the gravitational-wave signal from sound waves $\Omega_{\rm sw}$ and bubble collisions $\Omega_{\rm bc}$, arising from the LIGO-Virgo observing runs O1-O4a data. The previous analyses of this type in [98, 101] were based only on the O1-O3 data set. To this end, we perform a Bayesian analysis for the two cases (using `pygwb` [119]) assuming the priors on the parameters of the model and the CBC background specified in Table I. For the CBC background, we fix the power law index to $\alpha=2/3$ and we vary the amplitude $\Omega_{\rm ref}$.

Our analysis yields the Bayes factor $\ln\mathcal{B}^{\rm CBC+SW}_{\rm noise} = -0.647$ in the sound wave case, and $\ln\mathcal{B}^{\rm CBC+BC}_{\rm noise} =$

Parameter	Prior
$\alpha_{\rm PT}$	LogUniform$[10^{-2}, 10^{2}]$
$\beta/H_{\rm PT}$	LogUniform$[1, 10^{2}]$
$T_{\rm PT}$/GeV	LogUniform$[10^{5}, 10^{10}]$
$\Omega_{\rm ref}$	LogUniform$[10^{-13}, 10^{-6}]$
v_w	fixed at 1

TABLE I. Prior distributions assumed for the parameters of the model and the CBC background. For $\alpha_{\rm PT} \ll 1$ the gravitational-wave signal would be suppressed, while for $\alpha_{\rm PT} \gg 1$ the signal shape becomes independent from $\alpha_{\rm PT}$. The parameter $\beta/H_{\rm PT}$ cannot be less than 1 for consistency (see explanation in the text), while larger values suppress the gravitational-wave signal beyond detectability. The parameter $T_{\rm PT}$ is chosen such that the broken power law spectrum peak is at frequencies close to the ones accessible with LIGO-Virgo-KAGRA.

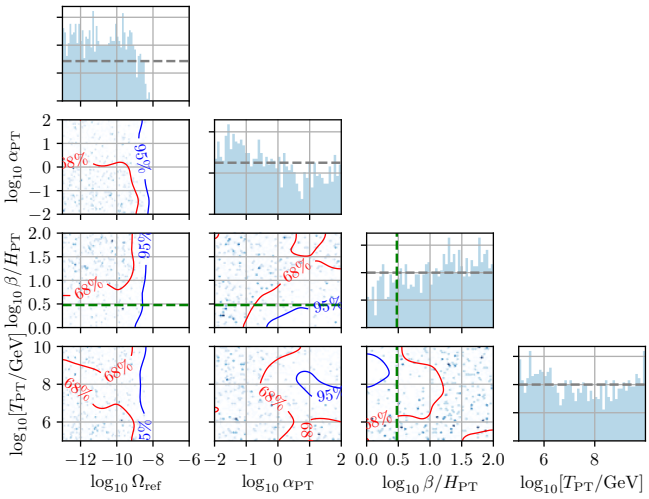

FIG. 2. Similarly as in Fig. 1, the constraints from the LIGO-Virgo observing runs O1-O4a data on the first order phase transition parameters including the CBC background, but for a dominant bubble collision contribution.

-0.679 for bubble collisions, indicating no evidence for a combined first order phase transition plus CBC background in the data.

Fig. 1 shows the posterior distributions for the combined CBC and first order phase transition search in the case of a dominant sound wave contribution. The 95% and 68% CL exclusion contours are highlighted. In the posterior distributions, we also show with a gray dashed line the LogUniform priors.

Similarly, Fig. 2 presents the constraints from the combined CBC and first order phase transition search for a dominant bubble collision contribution. As Fig. 2 demonstrates, with the priors listed in Table I, the data excludes at 95% CL part of the parameter space of the bubble collision dominated phase transitions, especially the region of $T_{\rm PT} \gtrsim 10^8\,{\rm GeV}$ and $\beta/H_{\rm PT} \lesssim 3$. We conclude that particle physics models predicting first order phase transitions are testable with the LIGO-Virgo-KAGRA data.

It is important to remark that small values of β are at the edge of the consistency with the description of the phase transition. Note that the bubble size is related to the β parameter as $R_*^{-3} \sim (1/8\pi)(\beta/v_w)^3$ [120], so we indicated with a green dashed line in Figs 1 and 2 the limit in which the size of the bubbles becomes comparable to the Hubble volume (see e.g. [121–123] for recent studies on this regime).

Our study is restricted to the two types of gravitational-wave spectra described in the previous subsection. Given the continuous developments in the prediction of the power law of the gravitational-wave background (particularly for bubble collisions) we have also repeated our analysis but with varying power law index, in the range indicated at the end of the previous section. The marginalization makes the constraining power of the data weaker and results in even weaker constraints on the parameters of the phase transition.

Note that our analysis sets a 95% CL upper limit on the amplitude of the CBC background, $\Omega_{\rm ref}$, of 2.0×10^{-9} and 2.3×10^{-9} for the sound wave and bubble collision cases, respectively. These values are compatible with the ones reported in [19].

III. COSMIC STRINGS

A. Motivation

Cosmic strings are topological defects in the Universe, that can be generated from spontaneous symmetry breaking of a global or gauge symmetry which has non-trivial winding of the vacuum manifold during cosmological phase transitions [34] via the Kibble-Zurek mechanism [35, 124–126]. The width of the cosmic strings is inversely proportional to the energy scale of the symmetry breaking, and is thus generally tiny, making these strings line-like. Formed mainly as super-horizon objects, these long strings intercommute and intersect to form a network of string loops. String loops oscillate due to their tension and shrink due to the emission of gravitational waves, Nambu-Goldstone bosons, or gauge bosons, depending on which coupling of the radiated particle to the string world-sheet is dominant.

One of the simplest string models is the axion string model, resulting from a spontaneous symmetry breaking of U(1) global symmetry. The QCD axion string, as a global string, is one of the well-motivated axion string models since QCD axions [127–135] could contribute to the dark matter relic abundance. Axion strings predominantly radiate Nambu-Goldstone bosons (axions), and thus gravitational waves radiated by axion strings are subdominant. A recent study [136] embeds the QCD axion string into the gauged global string model resulting from two subsequent spontaneous symmetry breakings of

global U(1) and gauge U(1) symmetries. The model contains both global strings and gauge strings, and the gauge string as a bound state of two types of global strings can either radiate gravitational waves or axions depending on whether the gauge coupling is significantly smaller than the gravitational coupling. Thus, it enriches the radiation channels from gauge strings. Without further assumption on the string model, in what follows, we only consider gauge strings for which gravitational-waves is the dominant radiation channel.

The evolution of the string loops in an expanding Universe eventually results in a scaling distribution, with loop sizes proportional to the cosmic time or the Hubble radius. At high frequencies, the gravitational-wave production is dominated by cusps, kinks, and kink-kink collisions. The dimensionless decay constant that characterizes the radiation power of gravitational waves from cusps, kinks, and kink-kink collisions can be estimated by

$$\Gamma_{\rm d} \equiv \frac{P_{\rm GW}}{G\mu^2} = \sum_i \frac{P_{{\rm GW},i}}{G\mu^2} \ , \tag{11}$$

where $G\mu$ is the string tension, and $i = \{{\rm c}, {\rm k}, {\rm kk}\}$ denotes cusp, kink, and kink-kink collision cases. Incoherent superpositions of these gravitational waves lead to a gravitational-wave background, the detection of which can be used to infer the energy scale of the symmetry breaking, and is thus an important target for gravitational-wave detectors.

This target has been previously searched for with LIGO's O1 [137] and O2 [138] data, and more recently with LIGO and Virgo's O3 data combined with previous O1 and O2 data [139]. It has also been searched for by pulsar timing array experiments [140–142], and remains an important source of gravitational-wave background for future space-based gravitational-wave detectors [143–145], and atomic interferometers [146].

B. Model

The gravitational-wave spectrum is

$$\Omega_{\rm CS}(f) = \frac{4\pi^2}{3H_0^2} f^3 \sum_i \int dz \int dl h_i^2 \frac{d^2R_i}{dzdl} \ , \tag{12}$$

where the index i runs over cusps, kinks and kink-kink collisions, l denotes the invariant loop length, z stands for the redshift, and $h_i = A_i(l,z) f^{-q_i}$, with $A_i = g_{1,i} G\mu l^{2-q_i}/[(1+z)^{q_i-1} r(z)]$, $r(z)$ the comoving distance of the loop, $q = 4/3, 5/3, 2$ respectively for cusps, kinks, and kink-kink collisions, and $g_{1,i} \approx 0.85, 0.29, 0.10$ correspondingly. For each type i, the burst rate per redshift and loop size is

$$\frac{d^2R_i}{dzdl} = \frac{\varphi_V(z)}{H_0^3(1+z)} \frac{2N_i}{l} n(l,t) \Delta_i \ , \tag{13}$$

where $\Delta_i = (\theta_m/2)^{3(2-q_i)}$, with $\theta_m \equiv [g_2 f(1+z) l]^{-1/3}$ and $g_2 = \sqrt{3}/4$, denotes the fraction of burst events that can be detected, $n(l,t)$ is the loop distribution function (the number of loops of size l at time t per loop size per volume), N_i is the number of burst events per loop oscillation time, and $\varphi_V(z) = H_0^3 dV(z)/dz$, with $V(z)$ the proper volume at redshift z.

The spectrum above includes only the contribution from sub-horizon string loops, though long strings can also emit gravitational waves. As long strings intercommute, they are building a small-scale structure, resulting in the emission of radiation [147, 148]. This additional contribution is generally sub-dominant as compared with that from string loops, hence usually neglected.

As in O3 studies [139], we consider three typical models of the string loop population $n(\gamma, z)$ in a scaling regime within a Friedmann-Lemaître-Robertson-Walker metric, where $\gamma = \ell/t$ is the dimensionless loop size, and derive constraints on each of them. Model A [149] and B [150] (called Model 2 and 3 respectively in O1 study) are based on results from numerical simulations of Nambu-Goto string networks (zero thickness strings with intercommutation probability equal to unity), wherein the former infers the loop production function and the latter obtains directly the loop distribution. The analytical modeling [151] of Model B considers also the effect of gravitational-wave back-reaction on the loops. Model B leads to a higher number of small loops than model A, leading to important consequences in the rate of gravitational-wave events we can detect and on the amplitude of the gravitational-wave background. Model C [152] is constructed to incorporate features of both model A and B. It assumes that the scaling loop distribution is a power-law, but leaves its slope unspecified. As in O3 study, we consider two different examples of model C by choosing parameters to reproduce A and B in radiation and matter eras. Model C-1 (respectively C-2) reproduces qualitatively the loop production function of model A (respectively B) in the radiation-dominated era and the loop production of model B (respectively A) in the matter-dominated era.

C. Constraints using O1-O4a LIGO-Virgo data

Following the O3 study [139], we carry out a Bayesian analysis with the same posterior as previously

$$p(G\mu|N_k) \propto \mathcal{L}(\hat{C}_a^{IJ}|G\mu, N_k) p(G\mu|I, N_k) \ , \tag{14}$$

where $\mathcal{L}(\hat{C}_a^{IJ}|G\mu, N_k)$ is the likelihood

$$\ln \mathcal{L} = -\frac{1}{2} \sum_{IJ,a} \frac{[\hat{C}_a^{IJ} - \Omega_{\rm CS}(f_a; G\mu, N_k)]^2}{\sigma_{IJ}^2(f_a)} \ , \tag{15}$$

$\hat{C}_a^{IJ} \equiv \hat{C}^{IJ}(f_a)$ and σ_{IJ} are, respectively, the cross-correlation estimator and the variance for the detector pair IJ, running over LIGO-Livingston & LIGO-Hanford, LIGO-Hanford & Virgo and LIGO-Livingston

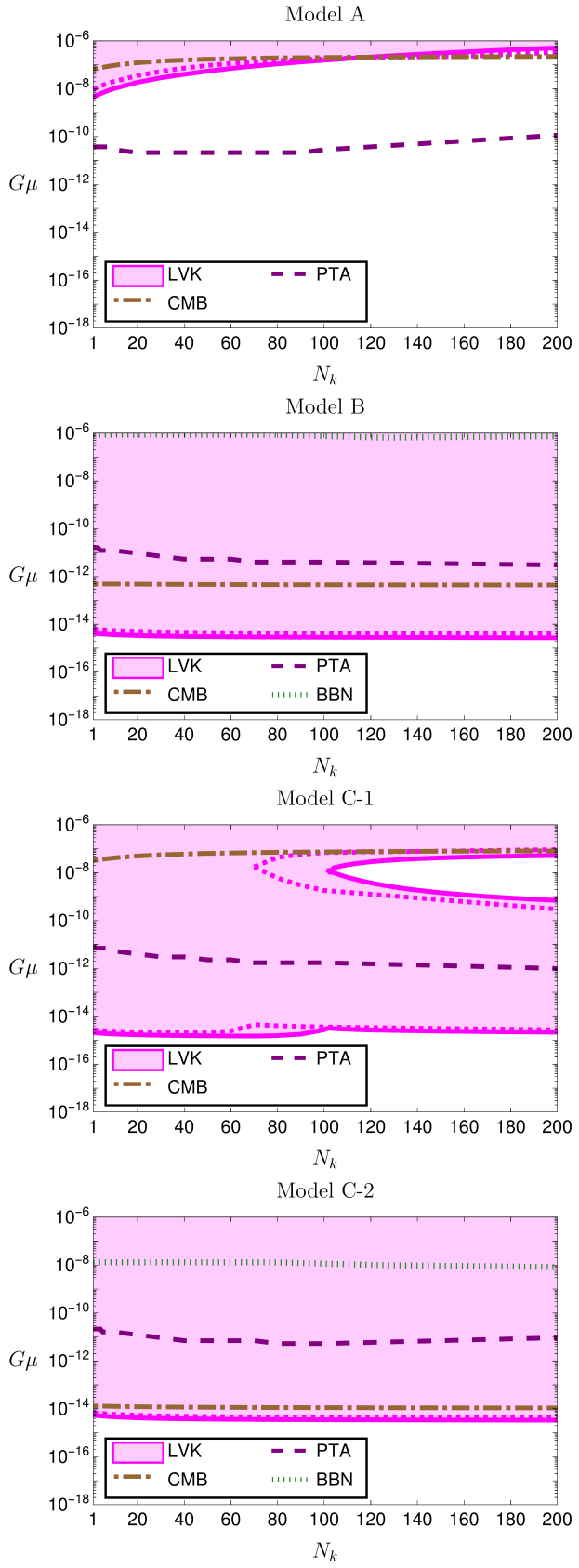

FIG. 3. Exclusion regions at the 95% CL on the cosmic string paramter space $(G\mu, N_k)$.

& Virgo [19]. The data used encompasses those used in O3 analysis, i.e., from O1, O2, and O3 runs, and in addition the data of LIGO-Livingston & LIGO-Hanford from the O4a period, while Virgo was not running during this period. In addition, $p(G\mu|I)$ is the prior on $G\mu$, and we impose a log-uniform prior for $G\mu$ in the range $10^{-18} \leq G\mu \leq 10^{-6}$, and do the analysis for each value of N_k, while fixing $N_c = 1$.

Since there is no detection, we show in Fig. 3 the exclusion region at the 95% CL on the parameters $G\mu$ versus N_k for the four loop distribution models, with O1, O2, O3 and O4a data.

Compared with previous results, the limits generally become stringent. For model A, the region $G\mu \gtrsim (4.5 \times 10^{-9} \sim 5.1 \times 10^{-7})$ is excluded for $1 \leq N_k \leq 200$, with the strongest constraint achieved at $N_k = 1$. This result improves over that of O1-O3 for a wide range of N_k. It becomes worse only for unrealistically high values of $N_k \geq 120$. More precisely, for $N_k < 120$, the constraint on $G\mu$ is better at most by a factor of about 0.47 while for $N_k \geq 120$ it is worse by at most 1.6.

For model B, the region $G\mu \gtrsim (2.7 \sim 4.2) \times 10^{-15}$ is excluded and this improves over that of O3 by a factor of 0.66 over the range of N_k considered here. For model C-1, the region $G\mu \gtrsim (1.5 - 3.2) \times 10^{-15}$ is excluded, and this improves on the previous result in all the range of N_k by a factor of $(0.33 \sim 0.79)$. Due to the features of the spectrum for this model, there is a region that cannot be excluded for higher values of $G\mu$. However, this region shrinks after the O4a data are included. For model C-2, the region $G\mu \gtrsim (3.4 \sim 5.5) \times 10^{-15}$ is excluded, which improves by a factor of 0.77 compared to O3.

It should be noted that the results presented here treat each choice of N_k as a separate model (with $N_c = 1$) in the Bayesian analysis. Increasing N_c has a similar effect as increasing N_k, as both lead to enhanced power of gravitational-wave emission, while the resulting changes to the constraints are different for the three models, with model A weakened, and model B and C less sensitive. Ideally, a joint distribution of N_k together with N_c should be used and a marginalization over these two parameters should be performed to obtain the constraint on $G\mu$. Due to a lack of simulations to get this information, we have adopted this approach. It should also be noted that the choice $\Gamma_d = 50$ is commonly used, according to simulation results. Enforcing this power emission corresponds to setting $(N_c, N_k) \approx (1, 9)$ or $(0, 18)$. The constraints for $(N_c = 0, N_k = 18)$ are slightly more stringent for most models except for C-1. This is due to the smaller value of Γ_d, despite the absence of gravitational-wave emission from cusps. More specifically, the excluded regions are $G\mu \gtrsim 9.2 \times 10^{-9}$ for model A, $G\mu \gtrsim 3.0 \times 10^{-15}$ for model B, $G\mu \gtrsim 2.6 \times 10^{-15}$ for model C1, and $G\mu \gtrsim 3.5 \times 10^{-15}$ for model C2.

In this analysis, the average number of cusps per oscillation on a loop has been set to 1. As it has been already shown in the O3 analysis [139], a high number of cusps gives qualitatively the same result as increasing the num-

ber of kinks. More precisely, numerical simulations have shown that the constraints are weakened for model A, whereas the bounds are insensitive to N_c for models B and C.

We include in Fig. 3 the corresponding constraints from pulsar timing arrays (PTA), Cosmic Microwave Background (CMB), and Big Bang Nucleosynthesis (BBN) obtained from the O3 analysis [139]. Note that these limits are obtained considering the nanohertz limit of the primordial background obtained from the Parkes Pulsar Timing Array [22] $\Omega_{\rm CS} < 2.3\times10^{-10}$ at a single frequency of 2.8×10^{-9} Hz, which is comparable to the latest results of NANOGrav, EPTA and ParkesParkes [140–142].

We briefly comment on the contribution from long strings [147, 153]. While generally subdominant for the case of Nambu-Goto strings [35, 143, 154, 155], they can provide the main contribution for Abelian-Higgs strings wherein simulations suggest the absence of stable string loops [156–159]. Moreover, recent works [160–162] suggest enhanced gravitational-wave production from long strings using a semi-analytic approach and a modeling of the kink structure with sharpness [163]. This makes the long string scenario potentially detectable by the LIGO-Virgo-KAGRA network. Adopting the spectrum from [162], we find that the excluded region is $G\mu \gtrsim 2.06 \times 10^{-7}$, comparable to the results obtained from the loop distribution of model A.

IV. DOMAIN WALLS

A. Motivation

In a cosmological context, domain walls (DWs) are two–dimensional defects that arise when a discrete symmetry is spontaneously broken during the thermal history of the Universe [35, 36]. Around the temperature of this symmetry–breaking phase transition, uncorrelated patches in space will select one among the possible disconnected degenerate vacua of the theory. DWs are then formed at the boundaries of those regions where the scalar field interpolates between different vacua. These field configurations are topologically stable owing to the underlying discrete symmetry. At the center of the DW, the field is trapped at the maximum of the scalar potential leading to a high energy density localized within the wall width. This results in a large DW tension, which is effectively the wall mass per unit surface. The relativistic motion of the DWs, driven by their own tension force or by vacuum pressure, acts as a powerful source of gravitational waves that can be detected today.

Similarly to other topological defects such as cosmic strings, DWs in the early Universe are known to reach a scaling regime with a constant $\mathcal{O}(1)$ number of walls per Hubble volume [37–42]. Differently from the strings, this implies that the relative importance of the DW network in the energy budget of the Universe grows with time, potentially leading to a phase of DW domination. As this is inconsistent with the standard evolution of the Universe, DWs have been often regarded as a cosmological problem. Crucially, however, a DW network is not expected to be absolutely stable, as the underlying discrete symmetry needs not to be exact but only approximate. In this case, DWs can annihilate before dominating the expansion of the Universe, leading to a strong gravitational-wave signal and no contradiction with standard cosmology.

New physics scenarios involving the formation of DWs are characterized by the presence of (approximate) discrete symmetries that are spontaneously broken in the early Universe. Relevant examples include the QCD axion [127–132, 164] and more generally axion–like particles, where a residual $\mathbb{Z}_N$ subgroup of the original U(1) Peccei–Quinn symmetry (we generally refer to U(1) Peccei-Quinn also for the case of axion–like particles that are not related to the strong CP problem) is left untouched by its chiral anomaly. This particular class of models implies the formation of cosmic strings at temperatures of the order of the axion decay constant, f_a, when the Peccei-Quinn symmetry is spontaneously broken and the axion is effectively massless. If this occurs after cosmic inflation, the strings and the corresponding inhomogeneous axion field will play an important role in the subsequent evolution of the system. In fact, as the axion mass increases while the Universe cools down, a network of axion DWs will ultimately form with each string attached to N walls of tension $\sigma_{\rm DW} \sim m_a f_a^2$, where m_a is the axion mass [165, 166]. The temperature of DW formation in this case can be estimated as the moment when the axion–like particle mass overcomes the Hubble friction, $m_a \sim H$.

The following dynamics depends on the value of N, which is referred to as the DW number. For $N = 1$ the string–wall network collapses very quickly after DW formation, as the theory actually possesses a unique vacuum. On the other hand, for $N > 1$ axion DWs are topologically stable and can be long–lived depending on the quality of the underlying Peccei-Quinn symmetry. This latter scenario is the one relevant for a gravitational-wave signal from DWs, as the string–wall dynamics is mostly controlled by the walls in this case.

Minimal QCD axion models predict the formation of DWs at temperatures around the QCD scale, $\Lambda_{\rm QCD} \sim 150\,$MeV, so that the corresponding gravitational waves would not overlap with the LIGO-Virgo-KAGRA observation band. Earlier formation of DWs leading to a detectable gravitational-wave signal is, however, possible for the so–called heavy QCD-axion models [167–169], which still solve the strong CP problem and ameliorate the issue with the quality of the U(1) Peccei-Quinn symmetry [170–175], or for general axion–like particles depending on the relevant scales [176].

Beyond the case of axions and axion–like particles, many other scenarios of new physics involve new discrete symmetries that can ultimately lead to the formation of a DW network. Well–motivated models include discrete flavor symmetries [177], left–right symmet-

ric models [178], supersymmetry [179–183], grand unification [184–186], and discrete spacetime symmetries [187].

B. Model

The dynamics of the DW network is controlled on one hand by the tension force, which tends to stretch the walls and reduce their surface to minimize the energy, and on the other hand by the Hubble expansion as well as the interaction of the walls with the primordial plasma. When particle friction can be neglected, DWs are known to approach a scaling regime in which the typical scale of the network, such as the average curvature and distance between the walls, is given by the Hubble radius, H^{-1}, indicating the presence of $\mathcal{O}(1)$ DWs per Hubble volume at any time [37–42]. In this regime, the energy density of the network is given by

$$\rho_{\rm DW} = 2\mathcal{A}\sigma_{\rm DW} H\,, \tag{16}$$

where $\mathcal{A} = \mathcal{O}(1)$ and $\sigma_{\rm DW}$ is the DW tension or mass per unit surface. Eq. (16) indicates that the energy density of the network decreases more slowly than matter or radiation, eventually leading to a DW–dominated epoch that is inconsistent with cosmological observations [36].

The temperature at which this would occur can be estimated by equating the energy density of the DWs to the critical density of the Universe, $\rho_c = 3H^2c^2/(8\pi G)$, yielding

$$T_{\rm dom} = \left(\frac{80\ G}{\pi c^4 g_*}\right)^{1/4} \sqrt{\sigma_{\rm DW}}\,, \tag{17}$$

where we have assumed radiation domination with g_* being the number of relativistic degrees of freedom.

Crucially, DW domination can be avoided if the underlying discrete symmetry is only approximate and the different vacua of the theory are actually biased by a small energy difference, ΔV, such that there exists only a unique true vacuum state [166, 188]. The microscopic origin of this bias will depend on the specific particle physics under consideration. However, according to the no global symmetry conjecture in quantum gravity [189–192], one expects the DW discrete symmetry to be ultimately broken at the Planck scale or earlier. In the case of axions and axion–like particles, the bias term can then descend from Planck–suppressed higher–dimensional operators that break the U(1) Peccei-Quinn symmetry as well as its $\mathbb{Z}_N$ subgroup relevant for DW formation.

The vacuum pressure resulting from the potential bias ΔV competes with the tension force trying to annihilate the DW network. The temperature at which the collapse initiates, $T_{\rm ann}$, can be estimated by equating the bias to the tension force or equivalently the DW energy density in the scaling regime, namely $\Delta V \sim \rho_{\rm DW}$, leading to

$$T_{\rm ann} \sim 10^8\ {\rm GeV} \left(\frac{10^{11}\ {\rm GeV}}{\sigma_{\rm DW}^{1/3}}\right)^{\frac{3}{2}} \left(\frac{\Delta V^{1/4}}{10^8\ {\rm GeV}}\right)^2 \left(\frac{100}{g_*}\right)^{\frac{1}{4}}. \tag{18}$$

For consistency, the annihilation temperature needs to be smaller than the temperature at which DWs form, which is at most as large as the DW tension $\sigma_{\rm DW}^{1/3}$ and parametrically suppressed for axion DWs. In the following we will hence restrict ourselves to $T_{\rm ann} \lesssim \sigma_{\rm DW}^{1/3}$.

During the lifetime of the DW network, gravitational waves are copiously produced by the relativistic motion of the walls [193–196]. As the energy density of the network actually increases with time compared to the critical density according to Eq. (16), the gravitational-wave emission is the strongest around the final time of DW annihilation. While the dynamics of the DW collapse itself can contribute to the emission of gravitational waves [197, 198], we will here consider only the gravitational-wave spectrum coming from the last period of scaling just before the collapse begins, namely at $T = T_{\rm ann}$. From numerical simulations [196], the energy density spectrum is found to be a broken power-law

$$\Omega_{\rm DW}(f) = \Omega_{\rm DW}^{\rm peak} \times \begin{cases} (f/f_{\rm peak})^3 & f < f_{\rm peak} \\ (f/f_{\rm peak})^{-1} & f > f_{\rm peak} \end{cases}, \tag{19}$$

where the peak amplitude associated to gravitational-wave emission at $T_{\rm ann}$ and red-shifted until today is given by

$$\Omega_{\rm DW}^{\rm peak} = 4.9\times10^{-6} \left(\frac{g_*}{100}\right) \left(\frac{g_{*s}}{100}\right)^{-\frac{4}{3}} \left(\frac{T_{\rm dom}}{T_{\rm ann}}\right)^4, \tag{20}$$

with g_{*s} the effective number of entropy degrees of freedom, and the red-shifted peak frequency is

$$f_{\rm peak} = 17\ {\rm Hz} \left(\frac{g_*}{100}\right)^{\frac{1}{2}} \left(\frac{g_{*s}}{100}\right)^{-\frac{1}{3}} \left(\frac{T_{\rm ann}}{10^8\ {\rm GeV}}\right). \tag{21}$$

In Fig. 4, we show a benchmark spectrum to highlight the effect of varying the DW tension, as well as the annihilation temperature.

C. Constraints using O1-O4a LIGO-Virgo data

We perform a Bayesian analysis following the approach described in Section I, and using the `pygwb` package [119]. For the gravitational-wave spectrum, we consider the contribution from a DW network, given by Eq.(19), in combination with the astrophysical gravitational-wave background from unresolved CBCs (defined as in Eq.(2) with $\alpha = 2/3$ and $f_{\rm ref} = 25$ Hz)

$$\Omega_{\rm GW}(f|\theta) = \Omega_{\rm DW}(f) + \Omega_{\rm CBC}(f)\,. \tag{22}$$

The parameters of interest are $\theta = (\Omega_{\rm ref}, \sigma_{\rm DW}, T_{\rm ann})$, with $\Omega_{\rm ref}$ the CBC background amplitude, and $T_{\rm ann}$ and $\sigma_{\rm DW}^{1/3}$ the parameters determining the cosmological gravitational-wave signal from DWs. The prior distributions for these parameters are summarized in Table II.

The resulting posterior distributions are shown in Fig. 5, which displays contour regions corresponding to

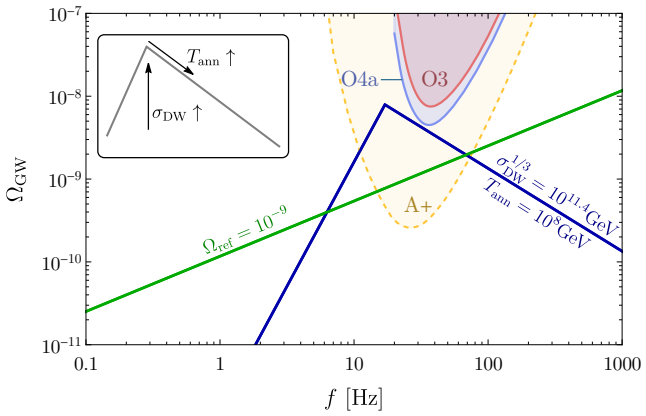

FIG. 4. The gravitational-wave spectrum of DW networks for a benchmark for the wall tension $\sigma_{\rm DW}$ and annihilation temperature $T_{\rm ann}$. The schematic in the top left box illustrates the impact of these parameters on the spectra: increasing the wall tension $\sigma_{\rm DW}$ enhances the peak amplitude, while a higher annihilation temperature $T_{\rm ann}$ reduces the amplitude and shifts the spectrum to higher frequencies. In addition, the assumed shape for the overlapping astrophysical gravitational wave background is displayed in green, for a representative value of $\Omega_{\rm ref}$ (and with $\alpha = 2/3$). Finally, sensitivity curves for LIGO-Virgo O3 run [68], as well as the ones of the O4a run [19] and LIGO A+ detector [199] are included.

Parameter	Prior
$\Omega_{\rm ref}$	LogUniform$[10^{-13}, 10^{-6}]$
$\sigma_{\rm DW}^{1/3}$/GeV	LogUniform$[10^{10}, 10^{13}]$
$T_{\rm ann}$/GeV	LogUniform$[10^{6}, 10^{10}]$

TABLE II. Prior distributions assumed for the parameters of the DW model and the CBC background. The prior on $\Omega_{\rm ref}$ comes from estimates of the CBC background [17], whereas the range for the priors on the tension $\sigma_{\rm DW}$ and the annihilation temperature $T_{\rm ann}$ are chosen large enough to include region of parameter space that would lead to gravitational-wave signals within the LIGO-Virgo-KAGRA observational band. Values for $T_{\rm ann}$ larger than $\sigma_{\rm DW}^{1/3}$ are not considered, as previously discussed around Eq.(18).

1 to 2σ CLs. From the posterior of the CBC background amplitude $\Omega_{\rm ref}$, we set an upper limit at the 95% CL, with a value 2.42×10^{-9}.

For the parameters controlling the DW signal, the region excluded by the gravitational-wave data is visualized in white in the bottom-middle panel. In the same panel, we have shaded in gray the values of $T_{\rm ann}$ and $\sigma_{\rm DW}$ for which the DW system would have dominated the Universe, leading to inconsistent cosmology. The excluded white region is close to DW domination, as the gravitational-wave signal is strongest when $T_{\rm ann} \sim T_{\rm dom}$. Our analysis can rule out annihilation temperatures in the range $10^7 \text{GeV} < T_{\rm ann} < 10^9 \text{GeV}$ for sufficiently large DW tension.

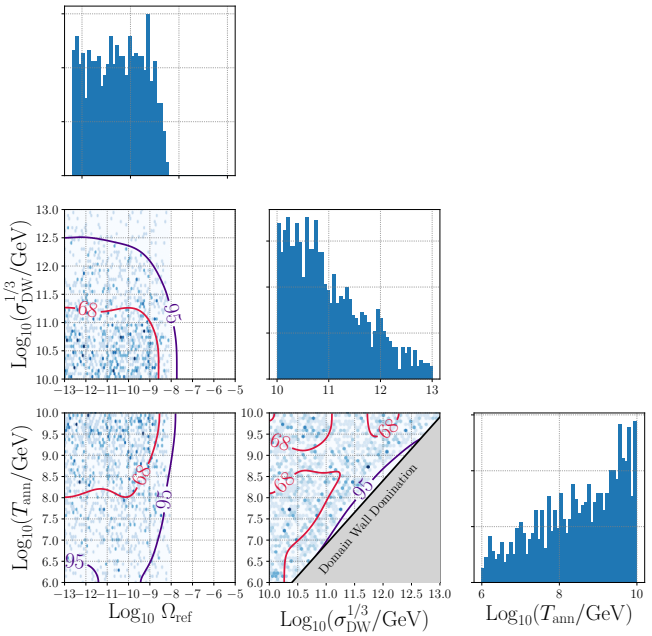

FIG. 5. Posteriors for the strength of the CBC background amplitude $\Omega_{\rm ref}$, the tension $\sigma_{\rm DW}$ of the DW network and the temperature $T_{\rm ann}$ at which the network annihilates using LIGO-Virgo data from O1, O2, O3 and O4a. The gray region in the bottom corresponds to a region where the DW network dominates the Universe, i.e. $T_{\rm ann} \leq T_{\rm dom}$.

Considering the hypothesis of a combined gravitational-wave background signal from a DW network and CBCs versus noise, the analysis yields a Bayes factor of $\ln \mathcal{B}^{\rm DW+CBC}_{\rm noise} = -1.15$, indicating no evidence for such a background in the data. Similarly, for a CBC-only background, we find $\ln \mathcal{B}^{\rm CBC}_{\rm noise} = -0.52$, implying a preference for the CBC-only scenario with $\ln \mathcal{B}^{\rm DW+CBC}_{\rm CBC} = -0.63$.

In conclusion, we find no evidence for a gravitational-wave signal from a DW network. The constraints on $\sigma_{\rm DW}$ and $T_{\rm ann}$ derived from gravitational-wave data exclude specific regions of parameter space, which can be used in the context of particle physics models.

V. STIFF EQUATION OF STATE

A. Motivation

Standard inflationary models in the slow roll regime typically give rise to a gravitational-wave background that is too weak to be detected by the current and future gravitational-wave experiments. Indeed, the current constraints on the scale of inflation and on the tensor-to-scalar ratio implies that the typical primordial gravitational-wave flat spectrum lies below the sensitivity of current and future gravitational-wave experiments in the ΛCDM model.

However, the detailed form of the primordial spectrum

and hence its detectability depends on the assumptions about the cosmological history in the period between reheating and the onset of BBN. In particular, adding an exotic era dominated by stiff energy (called the *stiff* dominated (SD) epoch, see e.g. [43–51]) leads to an inflationary gravitational-wave background growing at higher frequencies (i.e. blue tilted), making it accessible to the LIGO-Virgo-KAGRA network [50–53], future third generation detectors and space-based laser interferometer experiments [47, 200–210]. There are several concrete models in physics beyond the Standard Model that lead to cosmological periods with a stiff equation of state. We list here for instance quintessence models [43, 44, 211], axion scenarios [212–215], models with string theory moduli [216, 217], Peccei-Quinn inflation models [218], etc. In the following, we will introduce a model independent parametrization for a stiff epoch and explore the constraints imposed on this scenario by the O1 to O4a runs of LIGO-Virgo-KAGRA. The same model was previously constrained using the O1-O3 data in [53].

B. Model

The Universe can be described as a cosmological fluid with two key parameters: density ρ and pressure P. The equation of state parameter $w = P/\rho$ characterizes the Universe's behavior across different epochs. In the ΛCDM Model, inflation is immediately followed by a period of Radiation Domination (RD), with $w = 1/3$, then a period of Matter Domination (MD) with $w = 0$, and currently, a period of Dark Energy Domination with $w = -1$. Modifications to this sequence can be made by inserting other eras between the end of inflation and the onset of Big Bang Nucleosynthesis (BBN), provided the Universe is RD during BBN [46].

Our model introduces an unconventional sequence of epochs preceding the standard eras: an exotic RD era (denoted by RD1), an exotic MD era (denoted by MD1) and an exotic era driven by *stiff energy*, described by an equation of state parameter $1/3 \leq w_{\rm s} \leq 1$ (denoted by SD). The most extreme case of such a SD era is called kination, in which $w_{\rm s}$ is fixed to 1.

This cosmological model is motivated by high energy physics and can have a variety of observational consequences. Indeed, this specific sequence of epochs (in the case of kination) naturally arises in axion models [212–215] (see also [219–221]), providing a theoretical motivation for this cosmological scenario. In addition, a stiff era leads to a blue tilt in the inflationary gravitational-wave spectrum, making it observationally interesting. Finally, including a MD era suppresses the gravitational-wave spectrum at higher frequencies, allowing the model to evade indirect constraints from CMB and BBN observations.

The unconventional cosmological history enhances the inflationary gravitational-wave background, which results in a spectral shape with the following asymptotic behavior [53]

$$\Omega_{\rm SD}(f) = \Omega_{\rm SD}|^{(0)}_{\rm plateau} \begin{cases} \mathcal{A}_1 & \text{if} \quad f \ll f_{\rm RD} \\ \mathcal{A}_{\alpha_{\rm s}} \left(\frac{f}{f_{\rm RD}}\right)^{2(1-\alpha_{\rm s})} & \text{if} \quad f_{\rm RD} \ll f \ll f_{\rm SD} \\ \mathcal{A}_2 \left(\frac{f_{\rm SD}}{f_{\rm RD}}\right)^{2(1-\alpha_{\rm s})} \left(\frac{f_{\rm SD}}{f}\right)^2 & \text{if} \quad f_{\rm SD} \ll f \ll f_{\rm MD} \\ \mathcal{A}_1 \left(\frac{f_{\rm SD}}{f_{\rm RD}}\right)^{2(1-\alpha_{\rm s})} \left(\frac{f_{\rm SD}}{f_{\rm MD}}\right)^2 & \text{if} \quad f_{\rm MD} \ll f \end{cases} \tag{23}$$

with $\mathcal{A}_{\alpha_{\rm era}}$ a coefficient that depends on the equation of state at the moment when the gravitational-wave mode re-enters the Hubble radius, given by [46]

$$\mathcal{A}_{\alpha_{\rm era}} \equiv \frac{\Gamma^2(\alpha_{\rm era} + 1/2)}{\pi} \left(\frac{2}{\alpha_{\rm era}}\right)^{2\alpha_{\rm era}} , \; \alpha_{\rm era} \equiv \frac{2}{1 + 3w_{\rm era}} , \tag{24}$$

and where [50]

$$\Omega^{(0)}_{\rm SD}|_{\rm plateau} \equiv G_{\rm k} \frac{\Omega^{(0)}_{\rm rad}}{12\pi^2} \left(\frac{H_{\rm inf}}{M_{\rm Pl}}\right)^2 , \tag{25}$$

with $\Omega^{(0)}_{\rm rad} \approx 9 \times 10^{-5}$ and with $M_{\rm Pl} = 1/\sqrt{8\pi G} \approx 2.44 \times 10^{18}$ GeV the reduced Planck mass. Moreover, the factor $G_{\rm k} = [g_{*,\rm k}/g_{*,0}][g_{\rm s,0}/g_{\rm s,k}]^{\frac{4}{3}}$ encodes the change in relativistic degrees of freedom between today and the time when the mode k enters the Hubble radius at $k = aH$. The detailed gravitational-wave background assuming instantaneous transitions between subsequent epochs can be found in [53], and it is the one used in the following.

There are five different parameters that influence the spectrum, as can be seen in Fig. 6.

The Hubble scale of inflation $H_{\rm inf}$ influences the size of the spectrum. CMB polarization experiments Planck 2018, BICEP2, Keck Array and BICEP3 [222] constrain the tensor-to-scalar-ratio r and therefore also the inflationary power spectrum as $H_{\rm inf} < H_{\rm inf,max} = 5.12 \times 10^{13}$ GeV. The next-generation CMB experiment LiteBIRD [223] is expected to lead to an improvement in

this bound as $H_{\rm inf} < 1.21 \times 10^{13}$ GeV.

Then, $f_{\rm RD}$ is the frequency corresponding to the moment of transition between SD and RD2 and influences the position of the *elbow* between plateau and increase in spectrum (here RD2 denotes the standard radiation era occurring after the SD phase). Note that BBN should occur during the RD2 era, implying that $f_{\rm RD} \geq f_{\rm BBN} \simeq 1.41 \times 10^{-11}$ Hz.

Moreover, the equation of state parameter during the SD era, $w_{\rm s}$, determines the slope of the increasing part of the spectrum. The range for the related parameter $\alpha_{\rm s} \equiv 2/(1+3w_{\rm s})$ is $0.5 \leq \alpha_{\rm s} \leq 1$, where the lower bound corresponds to kination and the upper bound to radiation.

Then, $f_{\rm SD}$, which corresponds to the transition moment between MD1 and SD influences the peak amplitude and the location of the peak.

Lastly, $f_{\rm MD}$, which is the transition moment between RD1 and MD1 influences the elbow between the decreasing spectrum and the plateau on the right.

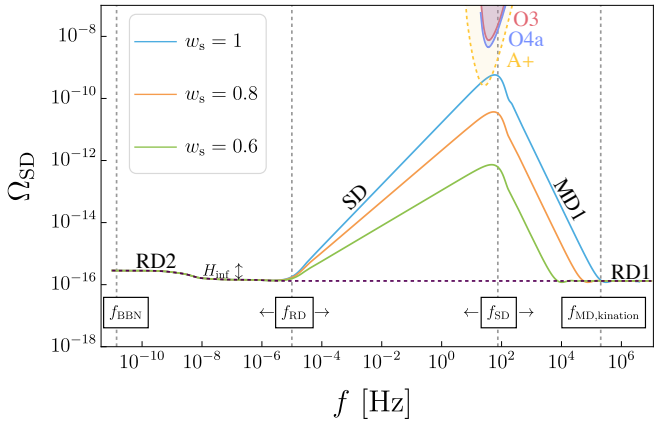

FIG. 6. The gravitational-wave background spectrum resulting from the exotic cosmology, for different choices of $w_{\rm s}$. The sensitivity curves for LIGO-Virgo O3 run [68], as well as the ones of the O4a run [19] and the LIGO A+ detector [199] are shown. The parameters that control the gravitational-wave spectrum are chosen as $H_{\rm inf} = H_{\rm inf,max}$, $f_{\rm RD} = 10^{-5}$ Hz, $f_{\rm SD} = 75$ Hz, and $f_{\rm MD}$ is fixed, so that the right plateau and the left plateau have the same amplitude. The standard inflationary gravitational-wave background is denoted with a purple dashed line. The parameter $H_{\rm inf}$ affects the overall gravitational-wave background amplitude, as indicated by the double arrow. The low-frequency part of the spectrum is shaped by $f_{\rm RD}$: lower values of $f_{\rm RD}$ shift the low-frequency plateau to the left, resulting in a stronger gravitational-wave background, while higher values shift it to the right, resulting in a weaker gravitational-wave background. The peak frequency of the spectrum depends on $f_{\rm SD}$: lower values shift the peak to the left (weaker gravitational-wave background), and higher values shift it to the right (stronger gravitational-wave background).

The gravitational-wave energy density can be constrained because of its contribution to the relativistic degrees of freedom in the Universe [23]. For the model considered here, we can estimate this bound as

$$\left(\frac{h^2\rho_{\rm GW}}{\rho_{\rm c}}\right)\Big|_{\tau=\tau_0} \approx \frac{1}{2(1-\alpha_{\rm s})} h^2\Omega_{\rm SD}(f_{\rm peak}) < 1.3\times10^{-6}\,, \tag{26}$$

where the right hand side is evaluated at the peak frequency $f_{\rm peak} \sim f_{\rm SD}$, and where we used the 2σ limit on $\Delta N_{\rm eff}$ from the CMB plus BBN analysis [224]. Further constraints on a stiff epoch could possibly arise from the enhancement of scalar modes [221], depending on the inflationary model.

C. Constraints using O1-O4a LIGO-Virgo data

We use the Bayesian analysis as described in Section I and employ the `pygwb` package [119]. The model for the gravitational-wave energy density spectrum $\Omega_{\rm GW}(f|\theta)$ combines the inflationary gravitational-wave background enhanced by a stiff era $\Omega_{\rm SD}(f)$ and the astrophysical gravitational-wave background from unresolved CBCs $\Omega_{\rm CBC}(f)$: $\Omega_{\rm GW}(f|\theta) = \Omega_{\rm SD}(f) + \Omega_{\rm CBC}(f)$. Within the relevant frequency range, the CBC background takes the form of Eq. 2 where $f_{\rm ref} = 25$ Hz is the reference frequency and $\Omega_{\rm ref}$ is the amplitude of the CBC background at this frequency, and we fix the power law to 2/3.

The parameter space is defined by $\theta = (\Omega_{\rm ref}, H_{\rm inf}, f_{\rm MD}, f_{\rm SD}, f_{\rm RD}, \alpha_{\rm s})$. For the Bayesian analysis, however, $H_{\rm inf}$ and $f_{\rm MD}$ are fixed by using delta function priors centered around a constant value. First, we fix $H_{\rm inf}$ to $H_{\rm inf,max} = 5.12 \times 10^{13}$ GeV, which maximizes the amplitude of the gravitational-wave signal. Note that, for the signal in the LIGO-Virgo-KAGRA observational frequency band, there is a degeneracy between $H_{\rm inf}$ and $f_{\rm RD}$, which could be used to translate the results presented here to another value of $H_{\rm inf}$ (for more details, see [53]). Second, we assume that $f_{\rm MD}$ is higher than the maximal frequency detectable with LIGO-Virgo-KAGRA. Specifically, notice that as soon as $f_{\rm MD} \gtrsim 100$ Hz, the high-frequency portion of the gravitational-wave spectrum, which is set by $f_{\rm MD}$, lies beyond the LIGO-Virgo-KAGRA observational band and therefore does not affect our analysis (see [53] for more details). For definiteness we set $f_{\rm MD} = f_{\rm i} = 1.8 \times 10^8$ Hz , where $f_{\rm i}$ represents the frequency associated with the end of inflation (assuming a constant Hubble scale during inflation and no entropy injection between RD1 and RD2). The priors for the other parameters are reported in Table III.

In our analysis, we concretely consider two scenarios:

- Kination Model: we fix $\alpha_{\rm s} = 0.5$, which corresponds to the maximum value for $w_{\rm s}$. This model is denoted as "kination+CBC" and its results are given in Fig. 7.

- General SD epoch Model: in this case $w_{\rm s}$ is allowed

Parameters θ	Prior
$\Omega_{\rm ref}$	LogUniform$[10^{-13}, 10^{-6}]$
$f_{\rm RD}$/Hz	LogUniform$[10^{-10}, 10^{-5}]$
$f_{\rm SD}$/Hz	LogUniform$[10^{-3}, 10^{6}]$
$\alpha_{\rm s}$	Uniform$[0.5, 1]$

TABLE III. Priors assumed for the Bayesian analysis. The prior for $\Omega_{\rm ref}$ comes from estimates of the CBC background [17]. The prior for α_s is determined by the allowed range of w_s: $1/3 \leq w_{\rm s} \leq 1$. The prior ranges for $f_{\rm RD}$ and $f_{\rm SD}$ are set to satisfy $f_{\rm BBN} \leq f_{\rm RD} < f_{\rm SD}$. They are selected over a sufficiently wide range to ensure that they include regions of parameter space leading to gravitational-wave signals within the LIGO-Virgo-KAGRA frequency band. We have verified that the posteriors are not significantly affected if we make the priors larger.

to vary, referred to as "SD+CBC". Its results are given in Fig. 8.

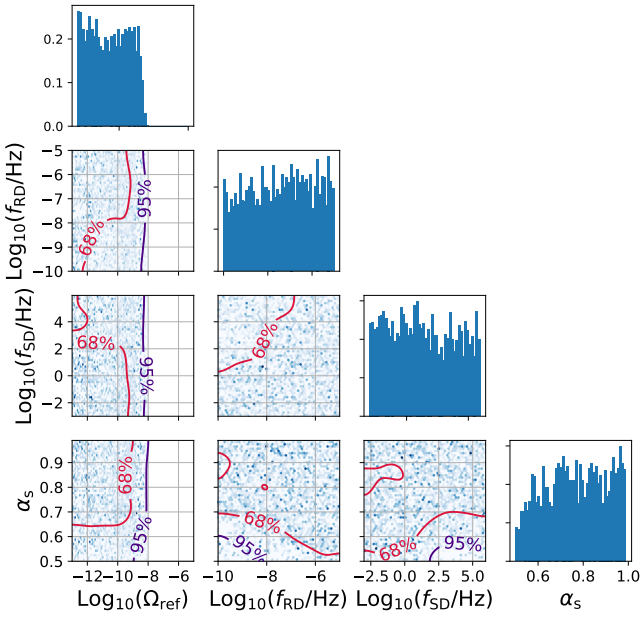

FIG. 7. Posteriors of the Bayesian analysis for an SD+CBC model. Contour regions in purple correspond to 95% CL and those in red to 68% CL.

Our study finds no evidence for either of these backgrounds, with log Bayes factors as follows: $\ln(\mathcal{B}^{\rm kination+CBC}_{\rm Noise}) = -1.16$ for the kination model, and $\ln(\mathcal{B}^{\rm SD+CBC}_{\rm Noise}) = -0.62$ for the model with varying $\alpha_{\rm s}$. We also compare a CBC-only background with a combined SD+CBC signal. For the kination model, we obtain $\ln(\mathcal{B}^{\rm kination+CBC}_{\rm CBC}) = -0.62$, suggesting a preference for a CBC-only background. For the general SD model, we find $\ln(\mathcal{B}^{\rm SD+CBC}_{\rm CBC}) = -0.09$, that indicates a small preference for a CBC background only.

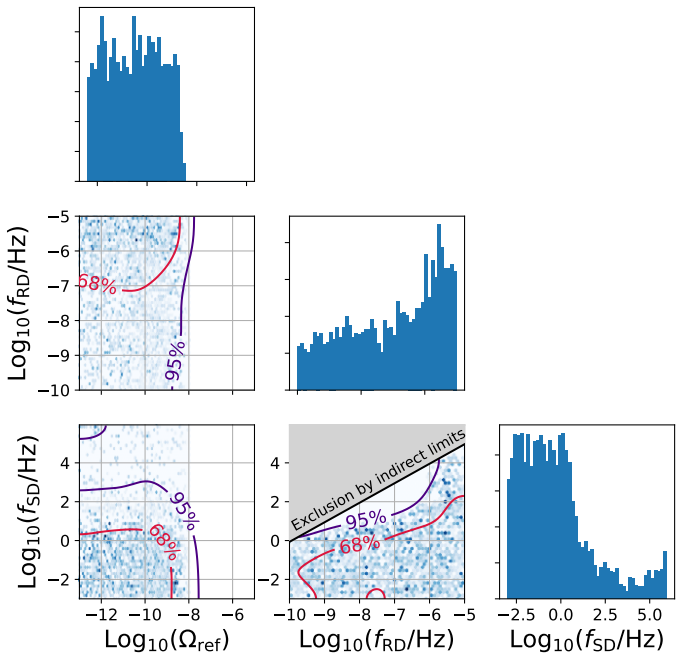

FIG. 8. Posteriors of the Bayesian analysis for the kination+CBC model. Here $\alpha_{\rm s}$ is fixed to $\alpha_{\rm s} = 0.5$. For the contour regions the same colors as in Figure 7 are used. The gray region in the bottom panel is excluded by indirect limits from BBN and CMB as in (26).

In summary, we do not find evidence in the O1 to O4a LIGO-Virgo data for either a CBC background or a gravitational-wave background coming from a stiff era. Consequently, we derive 95% CL upper limits on some of the parameters characterizing this unconventional cosmology. These are identified by the white regions in Fig. 7 and Fig. 8 (and slightly improve on the previous analysis performed only with O1-O3 data [53]). In Fig. 8, in the case of kination, we show that the data can exclude a portion of parameter space in the $f_{\rm RD}$ vs $f_{\rm SD}$ plane which would otherwise still be allowed by indirect limits. Our analysis, independently on the stiff epoch, also sets an upper limits on the amplitude of the astrophysical background, with value $\Omega_{\rm ref} \leq 2.9 \times 10^{-9}$.

VI. AXION INFLATION

A. Motivation

Gravitational waves offer a novel tool to test inflationary models and constrain their parameters. One inflationary model motivated by high energy physics is axion inflation, where a pseudo-scalar axion, coupled to a gauge field, leads to the early Universe accelerated expansion [54–57]. This model offers rich opportunities for cosmological observations [225, 226], including distinctive CMB features [227, 228], the formation of primordial

black holes [229] arising from the effective multi-field dynamics induced by the gauge field background, and a chiral gravitational-wave background [55, 230–233], which may be detectable by the LIGO-Virgo-KAGRA detectors.

Although U(1) gauge fields have been studied extensively, non-Abelian gauge fields, such as SU(2), present a compelling alternative. Their key difference is that the SU(2) gauge field can have an isotropic background value, whereas the U(1) cannot. As a result, gravitational-wave production can be computed using linear analysis in the case of SU(2), while it becomes a nonlinear process for U(1), generally requiring a more involved analysis to predict gravitational-wave amplitude [230, 234]. In our analysis, we focus on the SU(2) gauge field.

Gravitational waves can be efficiently produced when background gauge fields induce linear couplings between metric and tensor perturbations [235, 236]. While the original cosine inflaton potential is excluded by CMB observations [237, 238], other more complex models [232, 239–247] can evade CMB constraints and generate signals at currently detectable interferometric scales.

B. Model

We consider chromo-natural inflation [248, 249], for which the action reads [56, 248]

$$S = \int d^4x\sqrt{-\bar{g}}\Big[\frac{M_{\rm Pl}^2}{2}R - \frac{1}{2}(\partial\phi)^2 - V(\phi) - \frac{1}{4}F^a_{\mu\nu}F^{a\mu\nu} + \frac{\alpha_f}{4}\phi F^a_{\mu\nu}\tilde{F}^{a\mu\nu}\Big], \tag{27}$$

where $M_{\rm Pl}$ is the reduced Planck mass, $\bar{g} = \det(g_{\mu\nu})$, R denotes the Ricci scalar, ϕ is the inflaton axion field with a scalar potential $V(\phi)$. The SU(2) gauge field A^a_μ has field strength $F^a_{\mu\nu} = \partial_\mu A^a_\nu - \partial_\nu A^a_\mu - g\varepsilon^{abc}A^b_\mu A^c_\nu$, and its dual is $\tilde{F}^{a\mu\nu} = \varepsilon^{\mu\nu\rho\sigma}F^a_{\rho\sigma}/(2\sqrt{-\bar{g}})$. The axion–gauge coupling is denoted by α_f, and the gauge coupling by g.

We consider an isotropic ansatz for the homogeneous component of the gauge field,

$$A^a_0 = 0, \quad A^a_i = \delta^a_i a(t)Q(t), \tag{28}$$

where $Q \simeq (-\partial_\phi V/3\alpha_f g H)^{1/3}$ with $H \equiv \dot{a}/a$ the Hubble parameter [250–252].

The coupling between the inflaton and the SU(2) gauge field induces a tachyonic instability in one helicity mode of the gauge field. This leads to exponential amplification of that mode, which in turn sources a chiral (parity-violating) gravitational wave background [56, 238]. When the gauge coupling is small or the gauge field is weak, a non-Abelian SU(N) gauge theory behaves approximately like N^2-1 independent copies of an Abelian U(1) gauge theory. In the non-Abelian regime, the background gauge field acquires a nonzero vacuum expectation value (VEV), which enables a linear coupling between gauge field tensor perturbations and the metric tensor perturbations. This linear coupling allows the enhanced helicity +2 mode of the gauge field to efficiently source gravitational waves during inflation. In contrast, in the Abelian case, such couplings only arise at the nonlinear level, making the gravitational wave production less efficient. Therefore, we focus on the non-Abelian regime.

The gravitational wave background sourced in the non-Abelian regime can be analytically approximated as [246]

$$\Omega_{\rm SU(2)}(k) \simeq \frac{\sqrt{2}\Omega^{(0)}_{\rm rad}}{3}\Big(\frac{\xi^3 H}{\pi M_{\rm Pl}}\Big)^2_{\xi=\xi_{cr}}\Big(\frac{He^{(2-\sqrt{2})\pi\xi}}{g\sqrt{\xi}}\Big)^2_{\xi=\xi_{\rm ref}}, \tag{29}$$

where $\Omega^{(0)}_{\rm rad} = 9\times10^{-5}$ and $\xi = \alpha_f\dot{\phi}/2H$. In Eq. (29), the first term is evaluated at $\xi{\rm cr} = \xi(x=1)$, while the second term is evaluated at $\xi_{\rm ref} = \xi(x = (2+\sqrt{2})\xi_{\rm cr})$, with $x = -k\tau$ for conformal time τ. The non-Abelian regime is conservatively defined by the condition [246]

$$0.008e^{2.8\xi} \gtrsim 1/g\ . \tag{30}$$

A straightforward way to evade the CMB constraints is to consider the piecewise linear potential originally proposed by Starobinsky [253, 254],

$$V(\phi) = \begin{cases} V_0 + A_+(\phi-\phi_0), & \text{for } \phi > \phi_0 \\ V_0 + A_-(\phi-\phi_0), & \text{for } \phi < \phi_0 \end{cases}, \tag{31}$$

where V_0 sets the energy scale of the potential, and A_+ and A_- determine the slopes on either side of ϕ_0. Within the slow-roll approximation, the inflaton velocity remains approximately constant, leading to a constant velocity parameter ξ. This property greatly simplifies analytical calculations and facilitates the computation of the resulting gravitational-wave spectrum.

In Fig.9, we show the spectrum $\Omega_{\rm SU(2)}(k)$ for different parameter sets. Due to the constant velocity parameter ξ, the gravitational-wave amplitude remains constant over the relevant scales. We assume that the transition from the Abelian to the non-Abelian regime occurs near ϕ_0, positioned between CMB and interferometer scales, which determines where the enhanced gravitational-wave production begins. For further discussion of the allowed parameter space and analyses of alternative models, see [255].

Although the SU(2) gauge field can enhance gravitational waves during inflation, observational constraints exist, which we summarize below.

Cosmic Microwave Background: The Hubble expansion rate during inflation at the CMB scale, $H_{\rm CMB}$, sets the amplitude of the vacuum contribution to the gravitational-wave background, $\Omega_{\rm vac}(k) = \Omega^{(0)}_{\rm rad}H^2/(12\pi^2M_{\rm Pl}^2)$. The observable tensor-to-scalar ratio r is related to $H_{\rm CMB}$ through

$$H_{\rm CMB} = 2.7\times10^{14}r^{1/2}{\rm GeV}\,. \tag{32}$$

The latest observational constraint, $r < 0.036$ at 95% CL [222], translates into $H_{\rm CMB} < 2.1\times10^{-5}M_{\rm Pl}$, thereby ruling out certain classes of inflationary models.

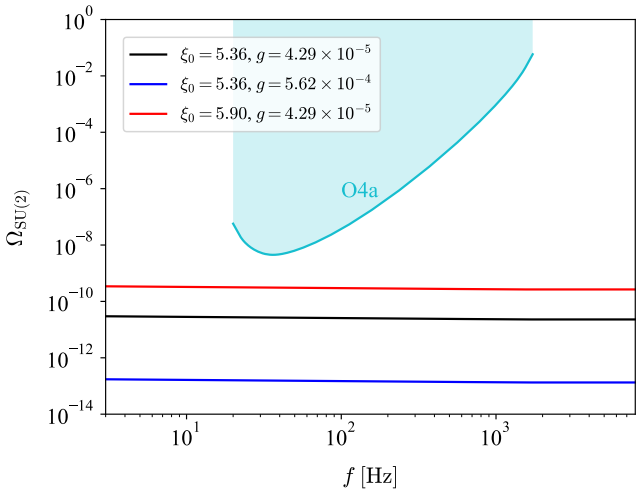

FIG. 9. Examples of Non-Abelian gravitational-wave background spectra for varying ξ_0, g, plotted with the O4a power-law integrated curve.

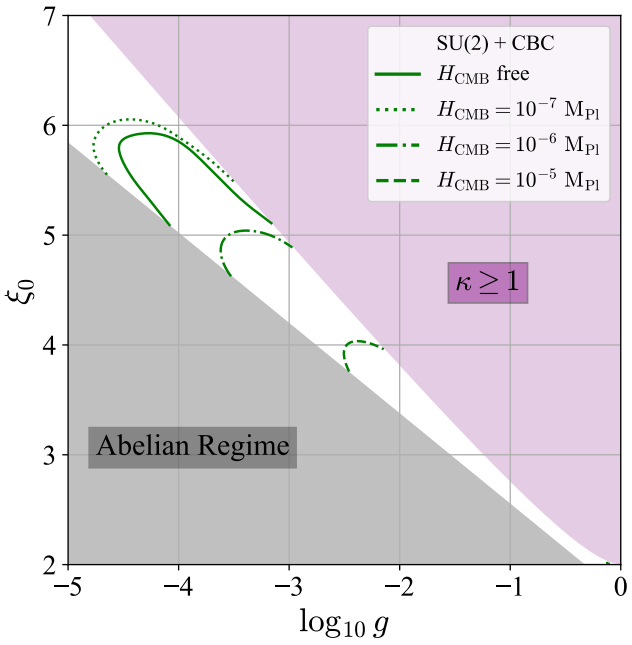

FIG. 10. Marginalized posterior in the $\xi_0 - \log_{10} g$ plane obtained from a search for early Universe axion inflation with an overlaid astrophysical background, assuming fixed values of $H_{\rm CMB} = 10^{-7}\ M_{\rm Pl}$, $10^{-6}\ M_{\rm Pl}$, $10^{-5}\ M_{\rm Pl}$ (dotted, dot-dashed, and dashed green lines, respectively), and also treating it as a free parameter (solid green line). The gray shaded region denotes the Abelian regime, where efficient gravitational-wave production is expected. The purple shaded region corresponds to the parameter space where strong back-reaction is anticipated, namely $\kappa \geq 1$, and the gravitational wave amplitude estimates may no longer be reliable.

Primordial Black Hole overproduction: Gauge-field–induced tensor modes can amplify primordial curvature fluctuations through second-order effects in cosmological perturbation theory. Once these fluctuations re-enter the Hubble radius, they may collapse into primordial black holes, whose abundance is tightly constrained by cosmological and astrophysical observations [256, 257]. If the curvature perturbations obey χ^2 statistics, primordial black hole formation is more efficient than in the Gaussian case, excluding a substantial region of parameter space [230]. This bound may however be alleviated in certain case. Lattice simulations of axion inflation with a U(1) gauge field suggest that, in the strong back-reaction regime, curvature perturbations approach a Gaussian distribution [258], reducing the expected primordial black hole abundance. While a similar analysis has not yet been carried out for SU(2) gauge field models, it is plausible that back-reaction effects could likewise relax primordial black hole constraints.

The strength of the back-reaction is controlled by the parameter κ [255, 259]

$$\kappa \simeq g\left(\frac{24\pi^2}{2.3e^{3.9m_Q}}\frac{m_Q^2}{1+m_Q^2}\right)^{-1/2}, \tag{33}$$

where $m_Q \equiv gQ/H$ plays the role of an effective mass. When back-reaction is an efficient mechanism, $\kappa \simeq 1$, the curvature perturbations would approach a Gaussian distribution and the primordial black hole constraint may be relaxed. However, if the back-reaction becomes too strong ($\kappa > 1$), the analytical expressions for the gravitational-wave spectrum are no longer reliable, and a dedicated numerical analysis would be required. We thus do not consider this latter case.

C. Constraints using O1-O4a LIGO-Virgo data

Parameter	Prior
$\Omega_{\rm ref}$	LogUniform$[10^{-12}, 10^{-7}]$
$N_{\rm CMB}$	Uniform$[50, 60]$
$f_0/{\rm Hz}$	LogUniform$[10^{-6}, 10]$
$\phi_{\rm end}/M_{\rm Pl}$	Uniform$[0, 25]$
$A_+/M_{\rm Pl}^3$	LogUniform$[10^{-20}, 10^{-6}]$
$A_-/M_{\rm Pl}^3$	LogUniform$[10^{-20}, 10^{-6}]$
$V_0/M_{\rm Pl}^4$	LogUniform$[10^{-20}, 10^{-6}]$
$\alpha_f/M_{\rm Pl}^{-1}$	Uniform$[0, 250]$
g	LogUniform$[10^{-5}, 1]$

TABLE IV. Prior distributions assumed for the parameters of the model and the CBC background.

We perform a Bayesian parameter estimation search for a combined non-Abelian and CBC background using `pygwb` [119]. The model has 8 free parameters and the

Parameters	$H_{\rm CMB}$ free	$H_{\rm CMB} = 10^{-5}\ M_{\rm Pl}$	$H_{\rm CMB} = 10^{-6}\ M_{\rm Pl}$	$H_{\rm CMB} = 10^{-7}\ M_{\rm Pl}$
$\Omega_{\rm ref}$	2.48×10^{-9}	3.18×10^{-9}	3.37×10^{-9}	2.72×10^{-9}
g	0.411	0.421	0.322	0.325
V_0	4.41×10^{-9}	2.36×10^{-10}	2.37×10^{-12}	2.50×10^{-14}
A_+	2.77×10^{-12}	3.73×10^{-11}	3.77×10^{-13}	3.69×10^{-15}
A_-	2.01×10^{-10}	1.60×10^{-11}	2.23×10^{-13}	2.36×10^{-15}
ξ_0	5.936	4.104	4.976	5.884
$H_{\rm CMB}/M_{\rm Pl}$	4.18×10^{-5}	-	-	-

TABLE V. 95% upper bounds on the SU(2)+CBC model and CBC background's parameters obtained under different Hubble constant $H_{\rm CMB}$ prior assumptions.

$H_{\rm CMB}$	$\log \mathcal{B}^{\rm GWB}_{\rm noise}$
Free	-0.515 ± 0.028
$10^{-7}\ M_{\rm Pl}$	-0.541 ± 0.029
$10^{-6}\ M_{\rm Pl}$	-0.555 ± 0.029
$10^{-5}\ M_{\rm Pl}$	-0.511 ± 0.028

TABLE VI. Parameter estimation log Bayes evidence factor for the searched combined model and CBC background under different Hubble constant $H_{\rm CMB}$ prior assumptions.

prior ranges are summarized in Table IV.

Figure 10 shows the 95% constraints obtained from the joint SU(2) + CBC analysis. We show both cases where all the 8 parameters are searched and where $H_{\rm CMB}$ is fixed at $H_{\rm CMB} = 10^{-5}M_{\rm Pl}, 10^{-6}M_{\rm Pl}, 10^{-7}M_{\rm Pl}$. The constraint is shown in the $\log_{10} g - \xi_0$ plane and other parameters are marginalized over. As discussed in the previous section, the viable region for ξ and g is limited to a certain area around the diagonal line in Fig. 10. The gravitational wave amplitude is proportional to g^{-2} and an exponentially increasing function of ξ_0 (see Eq. (29)), and it becomes larger toward the upper-left region of Fig. 10. Consequently, the gravitational-wave observations constrain the parameter space above the green lines.

The constraint is most sensitive to the value of $H_{\rm CMB}$, as it affects the overall amplitude. As we can see from the figure, we obtain tighter constraints on g and ξ_0 when $H_{\rm CMB}$ is large, and vice versa. We can also observe that, when $H_{\rm CMB}$ is left free and marginalized over, the constraint is relatively weak. This is because, due to our prior allowing very small $H_{\rm CMB}$ values, small $H_{\rm CMB}$ likely dominate the results when $H_{\rm CMB}$ is marginalized over. In other words, the constraints is endent on the prior of $H_{\rm CMB}$, and fixing $H_{\rm CMB}$ eliminates this ambiguity.

This result can be understood physically as follows. In Fig. 10, if we fix g and gradually increase ξ_0 from a small value, the energy transfer from the inflaton to the gauge field is initially too weak, keeping the system in the Abelian regime, where gravitational wave production remains inefficient. However, beyond a certain threshold, the non-Abelian nature of the gauge field becomes significant, leading to enhanced gravitational wave generation. However, if ξ_0 becomes too large, backreaction effects become dominant, violating the assumptions of our analysis, or the resulting gravitational-wave signal would contradict LIGO-Virgo observations, leading to exclusion.

The result presented here applies specifically to the form of the potential given in Eq. (31). Different inflationary potentials yield different gravitational-wave spectra, as the latter is determined by the evolution of the scalar field (namely, ξ evolves differently). We chose the double linear potential model because a linear potential leads to a constant solution for the velocity parameter ξ, and the two-stage inflation allows us to avoid concerns about CMB constraints. This provides a relatively simple picture in which the gravitational-wave spectrum is determined by the velocity parameter at the second stage, ξ_0. For discussions on cosine-type potentials and the R^2 potential, we refer the reader to [246, 255].

VII. SECOND-ORDER SCALAR PERTURBATIONS

A. Motivation

The scalar-induced gravitational-wave background, arising from large-amplitude primordial curvature perturbations, provides an observational test for probing directly the epoch of inflation [58]. This topic has recently gained significant attention due to its connection with primordial black holes [260, 261]. In scenarios where primordial curvature fluctuations are amplified during inflation, primordial black holes form through the collapse of extremely dense regions shortly after the corresponding modes enter the Hubble radius [262, 263]. Associated with this process, gravitational waves are sourced by the second-order terms of scalar perturbations, in the context of cosmological perturbation theory [59–63]. Thus, an upper bound on the gravitational-wave background can provide constraints on primordial curvature perturbations [264–267].

The amplification of the primordial curvature spectrum can be achieved through various mechanisms.

Within the framework of single-field inflation, this can occur via the Hilltop-type or running mass models [268, 269]. However, these models typically enhance curvature perturbations toward the end of inflation, resulting in high-frequency signals that are not accessible with the observational band of LIGO-Virgo-KAGRA detectors [270]. An ultra slow-roll phase, achieved through a plateau region in the inflationary potential [271–273], provides a flexibility to adjust the scale of enhancement. Another possibility is to consider multi-field inflation, which can predict enhanced curvature perturbations through mechanisms such as hybrid inflation with a tachyonic instability [274, 275] or turns in field space, corresponding to a bending of the inflationary trajectory [276, 277].

B. Model

Although extensive phenomenological studies have been conducted on the scalar-induced gravitational-wave background, we provide constraints based on the simplest assumptions: a log-normal spectral shape and a Gaussian distribution of the primordial curvature perturbations. The peak in the primordial curvature power spectrum is assumed to take the form [278]

$$\mathcal{P}_\zeta(k) = \frac{A}{\sqrt{2\pi}\Delta} \exp\left[-\frac{\ln^2(k/k_*)}{2\Delta^2}\right] . \tag{34}$$

It is defined by its position k_* with its width controlled by the parameter Δ and its amplitude characterized by A. In the $\Delta \to 0$ limit, Eq. 34 reduces to a Dirac delta function $\mathcal{P}_\zeta(k) = A\delta(\ln(k/k_*))$. The assumption for the primordial curvature power, Eq. 34, provides constraints in a model-independent manner and serves as a good approximation for many inflationary models. Furthermore, given the relatively narrow frequency band, our constraints are not sensitive to the detailed shape of the spectrum. Inflationary models typically predict an enhanced curvature perturbation spectrum over a wider range of scales, which can be well-approximated by a log-normal peak with a large width within the LIGO-Virgo frequency coverage.

In our analysis we focus on a Gaussian distribution for the primordial curvature perturbations. Non-Gaussianity can significantly modify the spectrum of the scalar-induced gravitational-wave background [279–285], however the precise form of non-Gaussianity depends on the inflation model and a general parametrization is lacking.

Hence, assuming a Gaussian distribution for the curvature perturbations, the energy-density spectrum of the scalar-induced gravitational-wave background can be computed using the approximate analytical expression [286, 287]

$$\begin{aligned}
&\Omega_{\rm Scalar}(k)h^2 \\
&\simeq 1.62\times10^{-5}\left(\frac{\Omega^{(0)}_{\rm rad}h^2}{4.18\times10^{-5}}\right)\left(\frac{g_*}{106.75}\right)\left(\frac{g_{*,\rm s}}{106.75}\right)^{-4/3} \\
&\times \frac{1}{12}\int_{-1}^{1}dx\int_{1}^{\infty}dy\ \mathcal{P}_\zeta\left(k\frac{y-x}{2}\right)\mathcal{P}_\zeta\left(k\frac{x+y}{2}\right)F(x,y)\ ,
\end{aligned} \tag{35}$$

where $\Omega^{(0)}_{\rm rad}$ is the present value of the energy density fraction of radiation, and g_* and $g_{*,\rm s}$ are the effective number of degrees of freedom for energy density and entropy density, respectively. The function $F(x,y)$ is given by

$$\begin{aligned}
F(x,y) &= \frac{288(x^2+y^2-6)^2(x^2-1)^2(y^2-1)^2}{(x-y)^8(x+y)^8} \\
&\times \left[\left(x^2-y^2+\frac{x^2+y^2-6}{2}\ln\left|\frac{y^2-3}{x^2-3}\right|\right)^2\right. \\
&+ \left.\frac{\pi^2}{4}(x^2+y^2-6)^2\theta(y-\sqrt{3})\right] ,
\end{aligned} \tag{36}$$

where θ denotes the Heaviside step function. The frequency range of our search corresponds to wavenumbers between approximately 10^{16} and $10^{19}\,\mathrm{Mpc}^{-1}$. These scales re-entered the Hubble horizon when the temperature exceeded $10^8\,\mathrm{GeV}$, allowing us to set $g_* = g_{*,\rm s} = 106.75$ within the Standard Model framework.

Figure 11 shows the spectrum assuming a log-normal curvature power spectrum for different values of the width parameter, $\Delta = 0, 0.1, 1$, while keeping A and k_* fixed. As Δ increases, the peak becomes broader and the spectral amplitude decreases. The integrated amplitude A sets the overall normalization, with the spectrum scaling as $\Omega_{\rm Scalar}(f) \propto A^2$, while the peak scale k_* determines the frequency at which the spectrum reaches its maximum.

The peak scale is set by the specific mechanism that enhances scalar perturbations during inflation, and the gravitational-wave spectrum peaks at approximately the same wavenumber as the curvature power spectrum. If primordial black holes form after the corresponding mode re-enters the Hubble radius, their mass can be related to the peak frequency as

$$\begin{aligned}
f_* \equiv \frac{ck_*}{2\pi} &= 25\left(\frac{k_*}{1.6\times10^{16}\ \mathrm{Mpc}^{-1}}\right)\mathrm{Hz} \\
&\simeq 25\ \gamma_H^{1/2}\left(\frac{M_{\rm PBH}}{5.3\times10^{-20}M_\odot}\right)^{-1/2}\mathrm{Hz}\,,
\end{aligned} \tag{37}$$

where $M_\odot \simeq 2\times10^{30}\,\mathrm{kg}$ is the solar mass, and $\gamma_H := M_{\rm PBH}/M_H$, typically of order unity, accounts for the difference between the primordial black hole mass $M_{\rm PBH}$ and the horizon mass M_H.

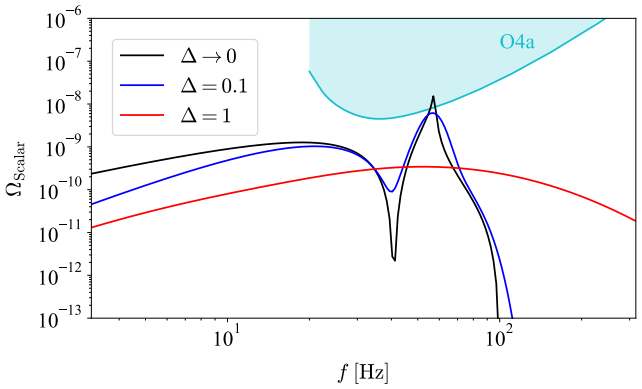

FIG. 11. Spectrum for different values of width $\Delta = 0, 0.1, 1$ plotted with the O4a power-law integrated curve. We assume $A = 0.01$ and $f_* = 50$Hz.

Parameter	Prior
$\Omega_{\rm ref}$	LogUniform$[10^{-13}, 10^{-5}]$
A	LogUniform$[10^{-6}, 10^{0.5}]$
f_*/Hz	LogUniform$[10^{-2}, 10^{6}]$
Δ	fixed at 0 and 1

TABLE VII. Prior distributions assumed for the parameters of the scalar-induced gravitational wave background and the CBC background.

C. Constraints using O1-O4a LIGO-Virgo data

The result of the Bayesian parameter estimation, obtained using `pygwb` [119], are shown in Fig. 12. The bounds set on A from the O4a data (shaded red region) are compared with BBN/CMB constraints for $\Delta \to 0$ and for $\Delta = 1$. The bottom and top horizontal axis represent the peak scale of the curvature perturbation k_* and the primordial black hole masses related with the scale calculated using Eq. (37), respectively. The shaded blue region represents indirect bounds from BBN/CMB on the abundance of the stochastic gravitational wave background. We calculate the bound by using the recent joint CMB+BBN analysis, which indicates that $\int d\ln f \; h^2\Omega_{\rm GW}(f) < 1.3 \times 10^{-6}$ at 2σ for $f > 2 \times 10^{-11}$Hz [224]. Since marginalized constraints tend to be prior dependent, here we run the Bayesian search by fixing the value of Δ and taking k_* and A as free parameters. The upper bound on A for different combinations of Δ and k_* are summarized in Table VIII.

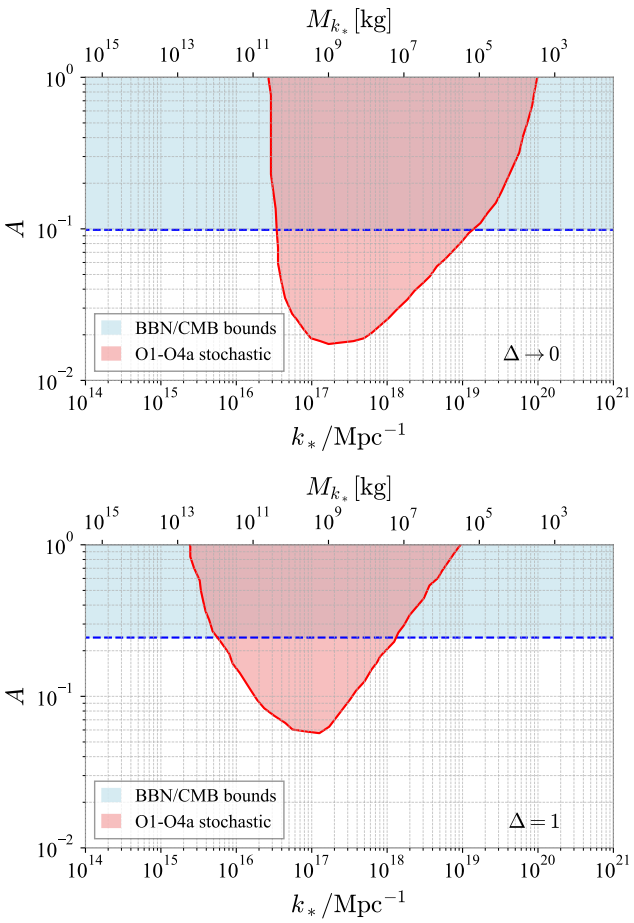

FIG. 12. Constraints on the curvature perturbation amplitude for $\Delta = 0$ (delta function case) and $\Delta = 1$.

	$k_* = 10^{15}\,{\rm Mpc}^{-1}$	$k_* = 10^{17}\,{\rm Mpc}^{-1}$	$k_* = 10^{19}\,{\rm Mpc}^{-1}$
$\Delta \to 0$	1.44	0.01	0.15
$\Delta = 1$	0.96	0.05	2.12

TABLE VIII. 95% CL Upper bounds on the power A of the curvature spectrum for fixed values of the peak position k_* and width Δ .

VIII. PRIMORDIAL BLACK HOLES

A. Motivation

Several mechanisms have been proposed for the formation of primordial black holes. One of the most extensively studied scenarios involves the amplification of small-scale perturbations during inflation. Other proposed mechanisms [64] include formation during phase transitions, an early matter-dominated era, scalar field instabilities, and the collapse of topological defects, among others. Their masses can span a wide range, from asteroid-like scales to supermassive sizes, depending on

the formation scenario. Primordial black holes are compelling candidates for dark matter [64, 288, 289] and may contribute to the observed population of binary black holes [290–298].

Just like astrophysical black holes, primordial black holes can form binaries and emit gravitational waves. The resulting gravitational-wave background, produced by a collection of unresolved events, provides a powerful probe of source populations in the early Universe [299–308]. Moreover, it offers a unique opportunity to test the existence of primordial black hole binaries, since the abundance of astrophysical black holes is expected to be low at high redshifts during the cosmic dark ages, before star formation. In contrast, primordial black holes could form binaries during this epoch, generating gravitational waves from the early Universe.

Here, two main formation channels are considered: one operating in the early Universe and another in the late Universe, as discussed in the following subsection. A key factor determining the merger rate is the number density of primordial black holes, typically quantified by $f_{\rm PBH}$, the fraction of dark matter composed of primordial black holes today. While current observations rule out $f_{\rm PBH} = 1$, primordial black holes could still make up a significant fraction of dark matter.

B. Model

The mass function of primordial black holes is commonly parametrized using monochromatic or log-normal distributions. This provides a good approximation for primordial black holes produced by a peak in the primordial power spectrum [309]. We define the log-normal mass function $p(m)$ as

$$p(m) = \frac{1}{\rho_{\rm PBH}} \frac{d\rho_{\rm PBH}}{d\ln m} \ , \tag{38}$$

where $\rho_{\rm PBH}$ stands for the primordial black hole energy density. For a log-normal distribution, the mass function takes the form

$$p(m) = \frac{1}{\sqrt{2\pi}\sigma} \exp\left[- \frac{(\ln m - \ln \mu)^2}{2\sigma^2} \right], \tag{39}$$

where μ is the median mass and σ controls the width of the distribution in logarithmic space. The mass function is normalized such that $\int p(m) d\ln m = 1$.

We calculate the gravitational-wave background generated by an ensemble of binary events by summing the energy spectra of individual binaries, considering the redshift of gravitational waves since emission and using the merger rate distribution [11]:

$$\Omega_{\rm PBH}(f) = \frac{f}{\rho_{c,0}} \int_0^{z_{\rm max}} dz \int d\ln m_1 \ d\ln m_2 \ \frac{p(m_1)p(m_2)}{(1+z)H(z)} \times \frac{d^2 R_{\rm EB/LB}}{d\ln m_1 d\ln m_2} \frac{dE_{\rm GW}}{df_{\rm r}} \ . \tag{40}$$

In Eq. (40) the integration is over the masses m_1 and m_2 of the binaries, and $f_{\rm r} = (1+z)f$ is the gravitational-wave frequency in the source frame. The quantity $d^2 R_{\rm EB/LB}/d\ln m_1/d\ln m_2$ represents the differential merger rate per unit time, comoving volume, and mass interval. Different binary formation mechanisms are denoted by EB (Early Binary) and LB (Late Binary). Early binaries form during the radiation-dominated era shortly after primordial black hole formation, while late binaries form later via dynamical capture in primordial black hole clusters during the matter-dominated era. We model the single-source energy spectrum $dE_{\rm GW}/df_r$ by the phenomenological fitting function of [310], which captures the inspiral, merger, and ringdown phases. Although binaries at high redshift emit gravitational waves early, the nearest binaries typically dominate the background power unless the merger rate rises sharply with redshift. Since the merger rate in our model does not increase steeply, we take $z_{\rm max} = 100$, which is sufficient to include all relevant contributions to the gravitational-wave background.

Several uncertainties may influence the shape of the gravitational-wave background, such as the binary formation mechanism and the potential disruption of binaries by a third body. The formation scenario can also affect properties like eccentricity, spin, and precession, which in turn modify the waveform. In what follows, we only consider non-spinning binaries.

The gravitational-wave background is composed of primordial black hole merger events occurring across a range of redshifts. If nearby binaries are the dominant ones, the spectrum exhibits a peak at the characteristic merger frequency, determined mainly by the primordial black holes masses. For equal-mass binaries, the energy spectrum has a peak at

$$f \simeq 8.3 \times 10^3 \left(\frac{M_{\rm PBH}}{M_\odot} \right)^{-1} {\rm Hz} \ . \tag{41}$$

Hence LIGO–Virgo–KAGRA detectors are sensitive to binaries with masses ranging from sub-solar scales up to $\mathcal{O}(10^2) M_\odot$. The possibility of probing such a background with the LIGO–Virgo–KAGRA detectors has been investigated in the literature [294, 301–303, 308, 311–313].

There are two major binary formation channels. In the Early Binary formation scenario, a binary originates from a pair of closely spaced primordial black holes, where the tidal influence of a third nearby object imparts the angular momentum necessary for binary formation. The merger rate for early binaries at cosmic time t is given by [291, 314–318]

$$\frac{d^2 R_{\rm EB}}{d\ln m_1 d\ln m_2} = \frac{1.6 \times 10^6}{{\rm Gpc^3 yr}} f_{\rm PBH}^{53/37} \left[\frac{t}{t_0} \right]^{-34/37} \times \left(\frac{m_1 + m_2}{M_\odot} \right)^{-32/37} \left[\frac{m_1 m_2}{(m_1+m_2)^2} \right]^{-34/37} \times S(m_1, m_2, f_{\rm PBH}), \tag{42}$$

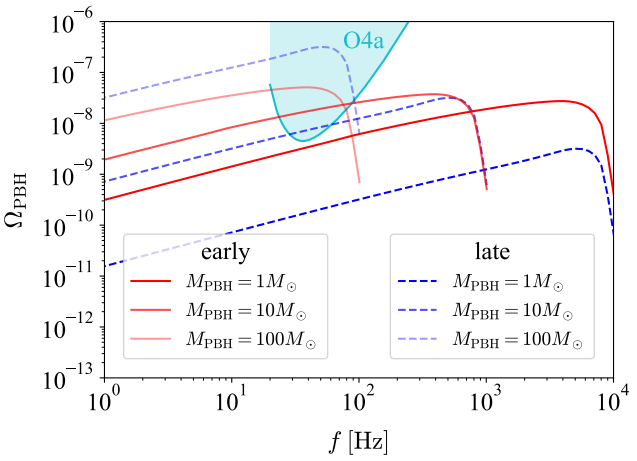

FIG. 13. Gravitational-wave background spectrum for monochromatic mass function, for both early (red solid) and late (blue dashed) binary formation channels. Different curves show different primordial black hole masses. We also plot the O4a power-law integrated curve. Here we assume $f_{\rm PBH} = 1$, fixed supression factor $S = 0.002$ and $R_{\rm clust} = 400$.

where t_0 is the age of the Universe. A rate suppression factor, S, has been introduced to take into account two main mechanisms that can suppress binary formation. One resulting from local matter inhomogeneities and nearby primordial black holes $S_1(m_1, m_2, f_{\rm PBH})$, and the other from clustering due to their initial Poissonian fluctuations $S_2(f_{\rm PBH})$ [293, 294, 318]. We employ suppression factors modeled with analytical methods [294, 318].

In the Late Binary formation senario, binaries can form within dense environments if clusters of primordial black holes develop during the matter-dominated era [290]. Analytical expressions for the merger rate can be derived by considering the two-body capture process within a cluster, under the assumption that the merger timescale of the resulting binary is much shorter than the age of the Universe [319, 320],

$$\frac{d^2 R_{\rm LB}}{d\ln m_1 d\ln m_2} = \frac{R_{\rm clust}}{\rm Gpc^3 yr} f_{\rm PBH}^2 \frac{(m_1+m_2)^{10/7}}{(m_1 m_2)^{5/7}} \,. \quad (43)$$

The parameter $R_{\rm clust}$ captures the enhancement of the primordial black hole merger rate due to local clustering [300, 321], which depends on their velocity dispersion and density contrast. We consider three representative values: $R_{\rm clust} = [1, 4\times10^2, 10^3]$, corresponding to (i) modest clustering consistent with ΛCDM [290], (ii) the level needed to match observed binary merger rates, and (iii) an optimistic scenario with highly efficient cluster formation [321].

With O4a sensitivity, the merger rate of late binaries is typically subdominant compared to early binaries, except for $m_{\rm PBH} \gtrsim 100, M_\odot$. This behavior is also illustrated in Fig. 13, which shows example spectra for both formation channels.

Parameter	Prior
$\Omega_{\rm ref}$	LogUniform$[10^{-12}, 10^{-7}]$
$\mu\,/M_\odot$	LogUniform$[10^{-1}, 10^{3}]$
σ	LogUniform$[10^{-2}, 1]$
$f_{\rm PBH}$	LogUniform$[10^{-5}, 1]$

TABLE IX. Prior distributions for the model parameters in Bayesian Analysis.

$R_{\rm clust}$	$\mu = 1\,[M_\odot]$	$\mu = 30\,[M_\odot]$	$\mu = 10^3\,[M_\odot]$
1	1.5×10^{-2}	3.7×10^{-3}	6.4×10^{-1}
4×10^2	1.6×10^{-2}	3.6×10^{-3}	4.5×10^{-1}
10^3	1.4×10^{-2}	3.8×10^{-3}	4.1×10^{-1}

TABLE X. 95% CL on $f_{\rm PBH}$ for various masses.

C. Constraints using O1-O4a LIGO-Virgo data

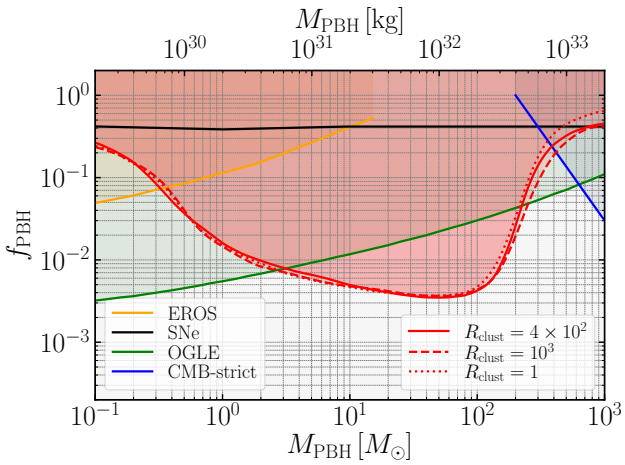

FIG. 14. The 95% CL constraints on $f_{\rm PBH}$ as a function of $M_{\rm PBH}$ $(= \mu)$ from the Bayesian analysis, shown for $R_{\rm clust} = 1, 4\times10^2, 10^3$ (dotted, solid, and dashed red curves). We also show other observational constraints such as supernova lensing constraints (SNe, black) [322] , Massive Compact Halo Object constraints (EROS, yellow) [323], the recent Optical Gravitational Lensing Experiment constraints (OGLE, green) [324], and Cosmic Microwave Background constraints (CMB, blue)[325].

The prior ranges for the parameters are summarized in Table IX. Note that we adopt relatively narrow prior for the width of the mass function σ, since the merger rate is known to be reliable only when the mass function is sharply peaked, particularly in the early binary formation scenario. The Bayesian analysis implies that no substantial gravitational-wave background sourced by primordial black holes or CBCs has been detected. We establish upper limits on the CBC energy density parameter $\Omega_{\rm ref} \sim 3\times10^{-9}$ at the 95% CL level, which are

consistent with the constraints from the isotropic background search [19].

Even in the absence of a detection, we can still constrain $f_{\rm PBH}$ as a function of μ. We show our constraint in Fig. 14, along with those from other analyses. Our constraint is derived by marginalizing over the mass function width σ and $\Omega_{\rm ref}$. For $M_{\rm PBH} \gtrsim 2\times10^2 M_\odot$, the spectral amplitude of the gravitational-wave background is predominantly attributed to the late binary formation channel. However, the O4a sensitivity loses its constraining power sharply in this mass range due to the limited frequency range. These findings underscore the ongoing and future importance of gravitational-wave background searches as a tool for probing phenomena within the mass range of $[1, 3\times10^2]\,M_\odot$. The resulting bounds are complementary to existing ones from individual binary events, microlensing surveys, and Cosmic Microwave Background observations. The posterior distributions of each parameter are shown in Fig. 15, and the 95% upper bound on $f_{\rm PBH}$ for various combinations of μ and $R_{\rm clust}$ are presented in Table X.

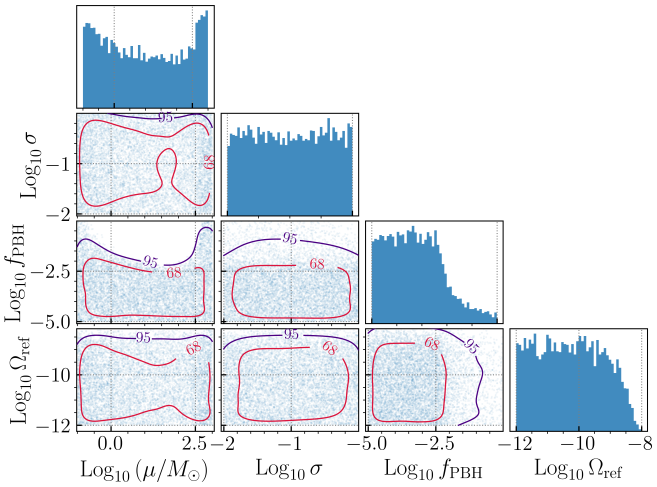

FIG. 15. Corner plots of the posterior distributions for the gravitational-wave background from primordial black hole binaries, assuming $R_{\rm clust} = 4\times10^2$. The results for other values of $R_{\rm clust}$ are very similar.

Lastly, we note that the parameters exhibit a degeneracy with the CBC contribution, $\Omega_{\rm ref}$, because both primordial and astrophysical sources produce a gravitational-wave spectrum with the same frequency dependence, $\propto f^{2/3}$, during the inspiral phase. This similarity is particularly relevant when the average black hole mass is $\lesssim 10M_\odot$. However, our results indicate the highest sensitivity to primordial black hole masses around $\sim 100M_\odot$, where the dominant contribution comes from the merger phase. In this regime, the spectrum has a characteristic frequency dependence, and its shape is sensitive to the assumed merger rate and mass distribution, allowing us to break the degeneracy between parameters.

IX. PARITY VIOLATION

A. Motivation

Several string-theory models and scalar-tensor models of gravity can result in circularly polarized gravitational waves, most notably models inspired by Chern-Simons gravity [326–329] and by inflationary scenarios coupled to Abelian gauge fields [330–335]. Chirality is also expected in various models of early Universe phase transitions [336–342] and axion inflation sourced by non-Abelian gauge fields, commonly referred to as chromo-natural inflation [56, 236, 246, 248, 343].

We describe a generic parity-violation search based on a power-law energy density gravitational-wave spectrum [65], then detail more theoretically motivated polarized gravitational-wave background models of early Universe turbulence and chromo-natural inflation.

B. Model

In searching for parity-violating models, we adopt the formalism [65] that uses modified cross-correlation estimator

$$\begin{aligned}\langle \hat{C}_{d_1 d_2}\rangle &= \int_{-\infty}^{\infty} df \int_{-\infty}^{\infty} df' \delta_T(f-f')\langle s^*_{d_1}(f) s_{d_2}(f')\rangle \tilde{Q}(f') \\ &= \frac{3H_0^2 T}{10\pi^2}\int_0^\infty df \frac{\Omega'_{\rm GW}(f)\gamma_I^{d_1 d_2}(f)\tilde{Q}(f)}{f^3}\,, \end{aligned} \tag{44}$$

where

$$\Omega'_{\rm GW} = \Omega_{\rm GW}\left[1+\Pi(f)\frac{\gamma_V^{d_1 d_2}(f)}{\gamma_I^{d_1 d_2}(f)}\right], \tag{45}$$

with

$$\begin{aligned}\gamma_I^{d_1 d_2}(f) &= \frac{5}{8\pi}\int d\hat{\Omega}(F^+_{d_1}F^{+*}_{d_2} + F^\times_{d_1}F^{\times *}_{d_2})e^{2\pi i f\hat{\Omega}\cdot\Delta\vec{x}}, \\ \gamma_V^{d_1 d_2}(f) &= -\frac{5}{8\pi}\int d\hat{\Omega}(F^+_{d_1}F^{\times *}_{d_2} - F^\times_{d_1}F^{+*}_{d_2})e^{2\pi i f\hat{\Omega}\cdot\Delta\vec{x}}\,. \end{aligned}$$

We denote T the measurement time, $\delta_T(f) = \sin(\pi f T)/(\pi f)$, $s_d(f)$ the strain time series of the two gravitational-wave detectors (denoted by d_1, d_2). $\tilde{Q}(f)$ is a filter and F_n^A stands for the contraction of the tensor modes of polarization $A = +, \times$ to the $n^{\rm th}$ detector's geometry. We denote by $\gamma_I^{d_1 d_2}$ the usual (unpolarized isotropic gravitational-wave background) overlap reduction function of detectors d_1, d_2 [76], and $\gamma_V^{d_1 d_2}$ as the overlap function associated with the parity violation term [344]. The polarization degree,

$$\Pi(f) = V(f)/I(f) = \frac{P_R(f)-P_L(f)}{P_R(f)+P_L(f)}\,, \tag{46}$$

ranges from -1 (fully left polarization) and 1 (fully right polarization), with $\Pi = 0$ corresponding to an unpolarized isotropic gravitational-wave background. We indicate by I, V the Stokes parameters and $P_{R/L}$ denote

the right- and left-hand gravitational-wave power spectra. Note that allowing $\Pi = 0$ in Eqs. (44), (46) returns the formalism to one utilized in standard, isotropic searches [19].

1. Model-independent

We conduct a generic search for a parity-violating gravitational-wave background exhibiting power-law behavior, Eq. (2), with $f_{\rm ref} = 25$ Hz. We use a log-uniform amplitude prior from 10^{-13} and 10^{-5}, while the model spectral index prior is a Gaussian distribution centered at 0 with a standard deviation of 3.5. We search for this model using the O1-O4a gravitational-wave data and place upper limits on its parameters.

We investigate both a simplified model with constant Π and a model in which the polarization varies with frequency. In the constant polarization case, we search uniformly for Π between -1 and 1. Additionally, two searches that fix $\Pi = -1$ and 1 are conducted to compare constraints under maximal chiral assumptions. For the frequency-dependent model, we use $\Pi(f) = \pm(f/1\ {\rm Hz})^{\beta}$ with a uniform prior β between -2 and 0. This is motivated from theoretical models where Π decays with increasing frequency [345, 346]. In our analysis we only consider frequencies larger than 1 Hz – at lower frequencies terrestrial detectors are limited by seismic noise – and hence the form of $\Pi(f)$ guarantees that the physically allowed bound $|\Pi| \leq 1$ is valid.

Parameter	Prior
$\Omega_{\rm ref}^{\rm PV}$	LogUniform$[10^{-13}, 10^{-5}]$
α	Gaussian$[0, 3.5]$
Π	Uniform$[-1, 1]$
β	Uniform$[-2, 0]$

TABLE XI. Prior distribution for the model-independent parity-violation searches.

2. Early Universe Turbulence

A parity-violating turbulent source during a phase transition will produce circularly polarized gravitational waves. Depending on the helicity strength, there are two types of turbulent gravitational-wave spectra [347, 348]. When energy dissipation at small scales dominates, it leads to a helical Kolmogorov spectrum, and we consider this type of polarization.

Parity violation at the electroweak scale can be realized in extensions of the Standard Model of particle physics, manifesting as helical (or chiral) turbulent motion [349, 350]. Circularly polarised gravitational waves are generated by parity-violating turbulent sources [351]. Their spectrum has a broken power-law spectrum with a peak at the characteristic frequency of the source. We search gravitational-wave data for models [352–354]

$$\Omega_{\rm Turbulence}(f) = \begin{cases} \Omega_{\rm peak}(f/f_{\rm peak}) & , \quad f \leq f_{\rm peak} \\ \Omega_{\rm peak}(f/f_{\rm peak})^{-8/3} & , \quad f > f_{\rm peak} \ . \end{cases} \tag{47}$$

The peak frequency $f_{\rm peak}$ is related to the temperature T_* at which the first-order phase transition takes place. At an energy scale of $T_* \sim 10^8$ GeV, the predicted chiral turbulence spectrum would exhibit a peak within the current LIGO-Virgo-KAGRA observational band. We therefore search for $f_{\rm peak}$ over a broad range $(10 - 2000)$Hz.

Previous numerical studies calculated the net circular polarization of gravitational waves under various initial turbulent conditions, determining the degree of polarization as a function of the wave number k. They identified models where Π depends on the frequency [345, 351]. We model the polarization as the power-law functional form described previously.

Parameter	Prior
$\Omega_{\rm peak}$	LogUniform$[10^{-13}, 10^{-5}]$
$f_{\rm peak}$/Hz	Uniform$[5, 2000]$
β	Uniform$[-2, 0]$

TABLE XII. Prior distribution for the turbulence parity-violation searches.

3. Non-Abelian Axion Inflation

The Chern-Simons interaction term sources exponential production of gravitational waves through the induced linear couplings between metric and gauge field tensor perturbations, and is given in Eq.(29).

The total gravitational-wave spectrum includes the vacuum contribution

$$\Omega_{\rm Vacuum}(k) = \frac{\Omega_{R,0}}{12\pi^2}\frac{H^2}{M_{\rm Pl}^2} \, . \tag{48}$$

We consider a piecewise linear model potential, given previously in Eq.(31). The inflaton velocity, in the slow-roll approximation, is approximately constant

$$\xi = \begin{cases} \xi_{\rm CMB} = A_+ \alpha_f / 2V_0, \ \text{for } \phi > \phi_0 \\ \xi_0 = A_- \alpha_f / 2V_0, \ \text{for } \phi < \phi_0 \ , \end{cases} \tag{49}$$

where CMB constraints set un upper bound of $\xi_{\rm CMB} < 2.5$ at 95% CL [355]. More studies for this model can be found in [254].

The Chern-Simons term not only sources significant production of gravitational waves, the spin-2 fluctuation of the gauge field leads to an asymmetry between its left- and right-handed polarization states. Thus, the gauge field can produce a chiral gravitational-wave signal within the ground detectors' frequency band.

In [235], it was shown that the enhanced helicity is model-dependent, and relies on the inflaton VEV sign;

right-handed tensor modes corresponding to positive VEV, left-handed modes for negative VEV. For the toy model studied, the polarization can be well approximated as

$$\Pi \simeq \frac{[\bar{\rho}_{\rm YM}/\bar{\rho}]\mathcal{G}_+^2(m_Q)}{[\bar{\rho}_{\rm YM}/\bar{\rho}]\mathcal{G}_+^2(m_Q)+1} = \text{const.} > 0 \ , \qquad (50)$$

where $\bar{\rho}_{\rm YM}/\bar{\rho} \lesssim \epsilon^2$ for slow-roll parameter ϵ, effective mass m_Q is approximated as $\xi \simeq m_Q + m_Q^{-1}$ and the explicit functional form of $\mathcal{G}_s(m_Q)$ is detailed in [235]. It is easy to show that $\Pi(f) \simeq 1$ for $\xi_0 \gtrsim 4$ and $\bar{\rho}_{\rm YM}/\bar{\rho} \gtrsim 5 \times 10^{-5}$ over the ground detectors' frequency band.

We perform a search for parity-violating axion inflation, a model investigated in Sec. VI by introducing an additional parameter for the polarization amplitude Π with a uniform prior range of $[0, 1]$. For the other parameters, we use the same prior range as in Table. IV. Note that we impose a non-negative prior on the polarization amplitude, as we expect $\Pi \geq 0$ for the studied toy model.

Parameter	Prior
$\Omega_{\rm ref}$	LogUniform$[10^{-13}, 10^{-5}]$
$N_{\rm CMB}$ [efolds]	Uniform$[50, 60]$
f_0/Hz	LogUniform$[10^{-6}, 10]$
$\phi_{\rm end}/M_{\rm Pl}$	Uniform$[0, 25]$
$A_+/M_{\rm Pl}^3$	LogUniform$[10^{-20}, 10^{-6}]$
$A_-/M_{\rm Pl}^3$	LogUniform$[10^{-20}, 10^{-6}]$
$V_0/M_{\rm Pl}^4$	LogUniform$[10^{-20}, 10^{-6}]$
$\alpha_f/M_{\rm Pl}^{-1}$	Uniform$[0, 250]$
g	LogUniform$[10^{-5}, 1]$
Π	Uniform$[0, 1]$

TABLE XIII. Prior distribution for the SU(2) axion inflation parity-violation searches. Note: the same as the previously listed prior table in Sec. VI, just with added Π prior.

C. Constraints using O1-O4a LIGO-Virgo data

We present the results for the models where a search was conducted. We find no evidence for parity-violation; constraints on such models are set.

1. *Model-independent*

We plot the results and the 65%, 95% confidence contours for the searched general models with an assumed CBC background in Figs. 16 and 17. Although no constraints can be placed on the parity-violating associated parameter, we set upper bounds on the background's strength parameter $\Omega_{\rm ref}^{\rm PV}$. We list the 95% upper bound on $\Omega_{\rm ref}^{\rm PV}$ and $\Omega_{\rm ref}$, plus the logarithmic Bayes factor for each general search in Table XIV.

Figure 18 displays the 68%, 95% confidence contours of the resulting $\Omega_{\rm ref}^{\rm PV} - \alpha$ posteriors from an assumed

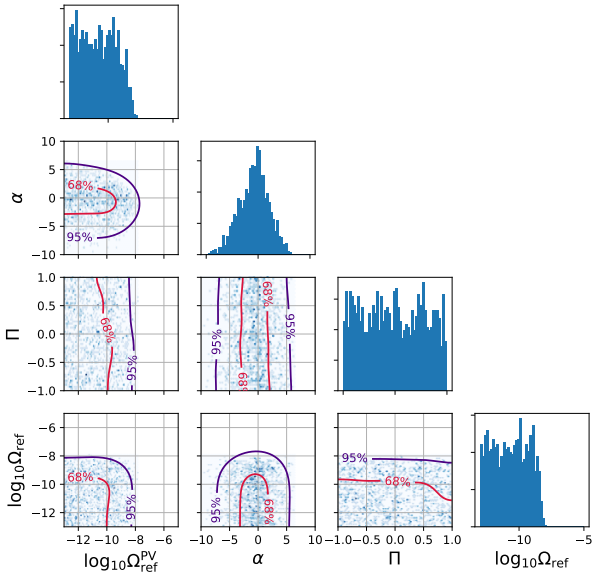

FIG. 16. Posterior distributions for a power-law gravitational-wave background model with $\Pi(f) = \text{const.}$, assuming an overlaying CBC background.

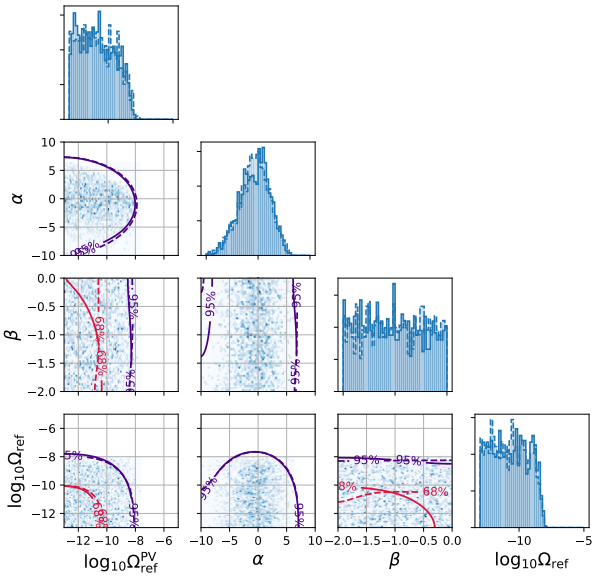

FIG. 17. Posterior distributions for a power-law gravitational-wave background model with $\Pi(f) = \pm(f/\text{Hz})^{\beta}$ (positive power-law in red, negative in purple) assuming an overlaying CBC background.

PV model	95% upper bound of $\Omega_{\rm ref}^{\rm PV}$	95% upper bound of $\Omega_{\rm ref}$	$\ln \mathcal{B}_{\rm noise}^{\rm PV\ Model+CBC}$
$\Pi = \text{const.}$	2.54×10^{-9}	2.61×10^{-9}	-1.175 ± 0.047
$\Pi = +(f/\text{Hz})^{\beta}$	2.41×10^{-9}	2.95×10^{-9}	-1.222 ± 0.043
$\Pi = -(f/\text{Hz})^{\beta}$	2.76×10^{-9}	2.46×10^{-9}	-1.203 ± 0.044

TABLE XIV. General parity-violating model search results with an assumed overlaying CBC background

.

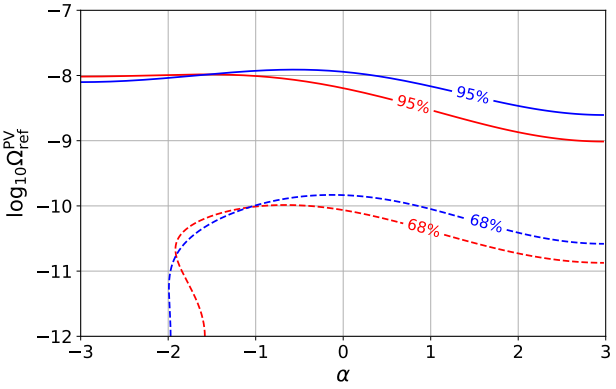

FIG. 18. $\Omega_{\rm ref}^{\rm PV} - \alpha$ confidence curve at 95% (solid) and 68% (dashed) level for assumed $\Pi = 1$ (red) and $\Pi = -1$ (blue) polarization.

$\Pi = \pm 1$ polarization. One can see that more stringent constraints can be made for an assumed entirely right-handed polarization ($2.82 \times 10^{-9} < \Omega_{\rm ref}^{\rm PV,95\%}$, red) than for a left-handed polarization ($2.94 \times 10^{-9} < \Omega_{\rm ref}^{\rm PV,95\%}$, blue); this was also found using the O3 data [356]. This preference can be explained by the ratio between the standard and parity-violating associated overlap reduction functions $\varsigma^{d_1 d_2} \equiv \gamma_V^{d_1 d_2}/\gamma_I^{d_1 d_2}$. While $\varsigma^{\rm HV}$ and $\varsigma^{\rm LV}$ are roughly periodic in the considered frequency range, $\varsigma^{\rm HL}$ is preferentially positive. Preferentially positive $\varsigma^{\rm HL}$ combined with $\Pi > 0$ results in enhanced modified $\Omega_{\rm GW}$ (Eq. (46)), hence leading to stricter constraints on right-hand polarized signals.

A general power-law search assuming no parity-violation ($\Pi = 0$) yields a logarithmic Bayes factor of $\ln \mathcal{B}_{\rm noise}^{\Pi=0+\rm CBC} = -1.194 \pm 0.042$. In combination with Table XIV, we find no statistical preference between polarized ($\Pi \neq 0$) and non-polarized ($\Pi = 0$) power-law models.

2. *Early Universe Turbulence*

We plot the resulting constraints from a parity-violating turbulence with overlaying CBC model search in Fig. 19. We calculate a log Bayes factor of $\log \mathcal{B}_{\rm noise}^{\rm Turb+CBC} = -0.830 \pm 0.035$, indicating no evidence for a chiral turbulent background. No constraints on

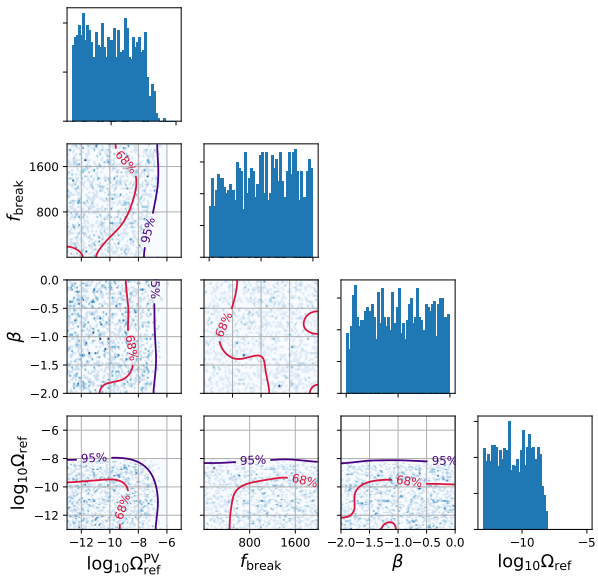

FIG. 19. Posterior distributions for early Universe turbulence with an overlaying CBC background model with $\Pi(f) = (f/\text{Hz})^{\beta}$.

parity-violating parameter β could be made. We find the 95% upper bound of the gravitational-wave background strength to be $\Omega_{\rm peak} < 5.39 \times 10^{-8}$ - larger compared to power-law background model constraints due to the allowed broken power-law spectra being able to peak at frequencies with poor sensitivity.

3. *Non-Abelian Axion Inflation*

We find a log Bayes factor of $\log \mathcal{B}_{\rm noise}^{\rm PV\ SU(2)+CBC} = -0.545 \pm 0.029$, and thus no evidence of such a model nor a preference for a polarized model over a non-chiral model. We list the 95% confidence limits on both searched models in Table XV, and there do not appear to be large discrepancies in the parameter estimation between the searched models. In Fig. 20, we show the 2D posterior $\xi_0 - H_{\rm CMB}$ results. Similarly, there are small differences between the searched models, highlighting the lack of statistical preference between chiral and

Parameter	$\Pi = 0$	$\Pi \neq 0$
g	0.411	0.385
$V_0/M_{\rm Pl}^4$	4.41×10^{-9}	3.47×10^{-9}
$A_+/M_{\rm Pl}^3$	2.77×10^{-12}	1.62×10^{-12}
$A_-/M_{\rm Pl}^3$	2.01×10^{-10}	2.55×10^{-10}
ξ_0	5.936	5.843
$H_{\rm CMB}/M_{\rm Pl}$	4.18×10^{-5}	3.94×10^{-5}
$\Omega_{\rm ref}$	2.48×10^{-9}	2.80×10^{-9}

TABLE XV. Parameter estimation 95% confidence upper bound for the searched chiral and non-chiral models.

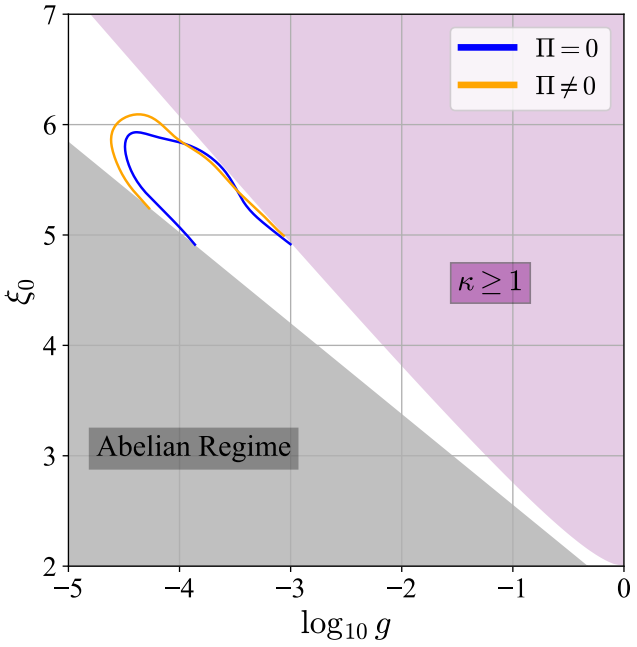

FIG. 20. Parameter estimation 95% confidence limit contours for the SU(2) gauge field model. The blue and orange curves show the 95% confidence limit contours for chiral ($\Pi \neq 0$) and non-chiral ($\Pi = 0$) searches.

non-chiral models. It is important to highlight that these results do not exclude other parity-violating models of axion inflation based on other scalar potential models.

X. CONCLUSIONS

The LIGO-Virgo-KAGRA collaboration uses the O4a data from LIGO Hanford and LIGO Livingston to search for a gravitational-wave background signal, in addition to the data from LIGO-Virgo from O1, O2 and O3. In this publication we report the results of dedicated searches of various particle physics models and cosmological scenarios which could contribute to the gravitational-wave background. These are first-order phase transitions, cosmic strings, domain walls, stiff equation of state, axion inflation, second-order scalar perturbations, primordial black holes, and parity violation. They can all lead to a gravitational-wave background potentially detectable by the LIGO-Virgo-KAGRA network.

First-order phase transitions could have occurred within the first one-trillionth of a second after the Big Bang, and their gravitational-wave imprints would be an important key to determining the correct theory beyond the Standard Model. They could generate gravitational waves from processes such as bubble collisions, sound waves propagating in the early Universe plasma, and magnetohydrodynamic turbulence. We place new constraints on the strength, temperature and duration of these transitions.

Cosmic strings are one-dimensional topological defects that can be generated after phase transitions followed by spontaneously symmetry breaking. Cosmic string loops oscillate because of their tension and shrink as a result of the emission of gravitational waves. We constrain the string tension, a parameter related to the temperature of the symmetry breaking. In particular, we exclude cosmic strings with a tension greater than $\mathcal{O}(10^{-15})$.

Domain walls are two-dimensional topological defects. Our analysis constrains the domain wall tension, and the temperature at which they collapse, resulting in their annihilation, to avoid domain wall dominance in the Universe. We rule out $10^7 \text{GeV} < T_{\rm ann} < 10^9 \text{GeV}$.

High energy physics can motivate a cosmological model with a stiff equation of state ($1/3 \leq w_{\rm s} \leq 1$). We derive 95% CL upper limits on some of the parameters characterizing this unconventional cosmology.

Gravitational waves offer a novel tool to test inflationary models and constrain their parameters. While single-field slow-roll inflation within the ΛCDM cosmological model predicts a gravitational-wave background that is too weak to be observed with current detectors, other inflationary models may produce a detectable gravitational-wave background. We consider an axion inflation model, where a pseudo-scalar axion is coupled to a gauge field and we impose constraints on the gauge coupling and the inflaton velocity.

The scalar-induced gravitational-wave background, arising from large-amplitude primordial curvature perturbations, provides an observational test for probing directly the epoch of inflation. In scenarios where primordial curvature fluctuations are amplified during inflation, primordial black holes form through the collapse of extremely dense regions shortly after the corresponding modes enter the Hubble radius. We impose an upper bound on a gravitational-wave background, leading to constraints on primordial curvature perturbations, stronger than the one imposed by Big Bang Nucleosynthesis and Cosmic Microwave Background at a scale of $\sim 10^{17}$Mpc.

Several mechanisms have been proposed for the formation of primordial black holes. Just like astrophysical black holes, primordial black holes can form binaries

and emit gravitational waves. A key factor determining the merger rate is the number density of primordial black holes, typically quantified by $f_{\rm PBH}$, the fraction of dark matter composed of primordial black holes today. We find 95% UL constraints on $f_{\rm PBH}$ as a function of the primordial black hole mass. In particular, we set $f_{\rm PBH} < 10^{-2}$ for primordial black holes with masses in the range $(1-100)M_{\odot}$.

Several string-theory models and scalar-tensor models of gravity can result in circularly polarized gravitational waves. We study a generic parity-violation search based on a power-law energy density gravitational-wave spectrum, then detail more theoretically motivated polarized gravitational-wave background models of early Universe turbulence and axion inflation. We impose new constraints on parity violation parameters.

In searching for a cosmologically produced gravitational-wave background, we also account for the presence of an astrophysical CBC background, composed of black holes and neutron stars. This is a background that LIGO–Virgo–KAGRA will likely detect before the cosmological background [15]. For the current generation of ground-based detectors, it will be challenging to separate astrophysical and cosmological contributions [357, 358]. Various methods have been proposed for signal separation with future detectors [359–363], such as the Einstein Telescope [364] and the Cosmic Explorer [365].

No gravitational-wave background signal has been detected for any of the cosmological and high energy physics models considered here, leading to constraints on their parameters. No CBC produced gravitational-wave background has been detected either. Nevertheless, our analyses demonstrate that the LIGO-Virgo data can already be used to derive new constraints on a variety of beyond the Standard Model theories, thereby enabling the testing of early Universe scenarios and particle physics models at energy scales otherwise inaccessible. We expect the constraints presented in this publication to be useful for particle physics and cosmological model building.

The LIGO–Virgo–KAGRA collaboration will continue to improve gravitational-wave background limits using data from the remainder of O4, with updated results to follow its completion. Although the sensitivity changes across O4a, O4b, and O4c are modest, the extended observing time will improve the sensitivity to the energy density of the gravitational-wave background. The subsequent O5 run will push these limits even further, deepening their impact on cosmology and high-energy physics.

ACKNOWLEDGMENTS

This material is based upon work supported by NSF's LIGO Laboratory, which is a major facility fully funded by the National Science Foundation. The authors also gratefully acknowledge the support of the Science and Technology Facilities Council (STFC) of the United Kingdom, the Max-Planck-Society (MPS), and the State of Niedersachsen/Germany for support of the construction of Advanced LIGO and construction and operation of the GEO 600 detector. Additional support for Advanced LIGO was provided by the Australian Research Council. The authors gratefully acknowledge the Italian Istituto Nazionale di Fisica Nucleare (INFN), the French Centre National de la Recherche Scientifique (CNRS) and the Netherlands Organization for Scientific Research (NWO) for the construction and operation of the Virgo detector and the creation and support of the EGO consortium. The authors also gratefully acknowledge research support from these agencies as well as by the Council of Scientific and Industrial Research of India, the Department of Science and Technology, India, the Science & Engineering Research Board (SERB), India, the Ministry of Human Resource Development, India, the Spanish Agencia Estatal de Investigación (AEI), the Spanish Ministerio de Ciencia, Innovación y Universidades, the European Union NextGenerationEU/PRTR (PRTR-C17.I1), the ICSC - CentroNazionale di Ricerca in High Performance Computing, Big Data and Quantum Computing, funded by the European Union NextGenerationEU, the Comunitat Autonòma de les Illes Balears through the Conselleria d'Educació i Universitats, the Conselleria d'Innovació, Universitats, Ciència i Societat Digital de la Generalitat Valenciana and the CERCA Programme Generalitat de Catalunya, Spain, the Polish National Agency for Academic Exchange, the National Science Centre of Poland and the European Union - European Regional Development Fund; the Foundation for Polish Science (FNP), the Polish Ministry of Science and Higher Education, the Swiss National Science Foundation (SNSF), the Russian Science Foundation, the European Commission, the European Social Funds (ESF), the European Regional Development Funds (ERDF), the Royal Society, the Scottish Funding Council, the Scottish Universities Physics Alliance, the Hungarian Scientific Research Fund (OTKA), the French Lyon Institute of Origins (LIO), the Belgian Fonds de la Recherche Scientifique (FRS-FNRS), Actions de Recherche Concertées (ARC) and Fonds Wetenschappelijk Onderzoek - Vlaanderen (FWO), Belgium, the Paris Île-de-France Region, the National Research, Development and Innovation Office of Hungary (NKFIH), the National Research Foundation of Korea, the Natural Sciences and Engineering Research Council of Canada (NSERC), the Canadian Foundation for Innovation (CFI), the Brazilian Ministry of Science, Technology, and Innovations, the International Center for Theoretical Physics South American Institute for Fundamental Research (ICTP-SAIFR), the Research Grants Council of Hong Kong, the National Natural Science Foundation of China (NSFC), the Israel Science Foundation (ISF), the US-Israel Binational Science Fund (BSF), the Leverhulme Trust, the Research Corporation, the National Science and Technology Council (NSTC), Taiwan, the United States Department of Energy, and the Kavli Foundation. The authors gratefully acknowl-

edge the support of the NSF, STFC, INFN and CNRS for provision of computational resources.

This work was supported by MEXT, the JSPS Leading-edge Research Infrastructure Program, JSPS Grant-in-Aid for Specially Promoted Research 26000005, JSPS Grant-in-Aid for Scientific Research on Innovative Areas 2402: 24103006, 24103005, and 2905: JP17H06358, JP17H06361 and JP17H06364, JSPS Core-to-Core Program A. Advanced Research Networks, JSPS Grants-in-Aid for Scientific Research (S) 17H06133 and 20H05639, JSPS Grant-in-Aid for Transformative Research Areas (A) 20A203: JP20H05854, the joint research program of the Institute for Cosmic Ray Research, University of Tokyo, the National Research Foundation (NRF), the Computing Infrastructure Project of the Global Science experimental Data hub Center (GSDC) at KISTI, the Korea Astronomy and Space Science Institute (KASI), the Ministry of Science and ICT (MSIT) in Korea, Academia Sinica (AS), the AS Grid Center (ASGC) and the National Science and Technology Council (NSTC) in Taiwan under grants including the Science Vanguard Research Program, the Advanced Technology Center (ATC) of NAOJ, and the Mechanical Engineering Center of KEK.

[1] J. Aasi *et al.* (LIGO Scientific), Class. Quant. Grav. **32**, 074001 (2015), arXiv:1411.4547 [gr-qc].
[2] F. Acernese *et al.* (VIRGO), Class. Quant. Grav. **32**, 024001 (2015), arXiv:1408.3978 [gr-qc].
[3] T. Akutsu *et al.* (KAGRA), PTEP **2021**, 05A101 (2021), arXiv:2005.05574 [physics.ins-det].
[4] A. G. Abac *et al.* (LIGO Scientific, VIRGO, KAGRA), arXiv (2025), arXiv:2508.18079 [gr-qc].
[5] A. G. Abac *et al.* (LIGO Scientific, VIRGO, KAGRA), arXiv (2025), arXiv:2508.18082 [gr-qc].
[6] A. G. Abac *et al.* (KAGRA, Virgo, LIGO Scientific), Phys. Rev. Lett. **135**, 111403 (2025), arXiv:2509.08054 [gr-qc].
[7] B. P. Abbott *et al.* (LIGO Scientific, Virgo, 1M2H, Dark Energy Camera GW-E, DES, DLT40, Las Cumbres Observatory, VINROUGE, MASTER), Nature **551**, 85 (2017), arXiv:1710.05835 [astro-ph.CO].
[8] B. P. Abbott *et al.* (LIGO Scientific, Virgo), Phys. Rev. Lett. **119**, 161101 (2017), arXiv:1710.05832 [gr-qc].
[9] N. Christensen, Rept. Prog. Phys. **82**, 016903 (2019), arXiv:1811.08797 [gr-qc].
[10] J. C. N. de Araujo, O. D. Miranda, and O. D. Aguiar, Phys. Rev. D **61**, 124015 (2000), arXiv:astro-ph/0004395.
[11] E. S. Phinney, arXiv (2001), arXiv:astro-ph/0108028.
[12] T. Regimbau and J. A. de Freitas Pacheco, Astrophys. J. **642**, 455 (2006), arXiv:gr-qc/0512008.
[13] T. Regimbau, Res. Astron. Astrophys. **11**, 369 (2011), arXiv:1101.2762 [astro-ph.CO].
[14] A. C. Jenkins, R. O'Shaughnessy, M. Sakellariadou, and D. Wysocki, Phys. Rev. Lett. **122**, 111101 (2019), arXiv:1810.13435 [astro-ph.CO].
[15] R. Abbott *et al.* (KAGRA, Virgo, LIGO Scientific), Phys. Rev. D **104**, 022005 (2021), arXiv:2103.08520 [gr-qc].
[16] B. P. Abbott *et al.* (LIGO Scientific, Virgo), Phys. Rev. Lett. **116**, 131102 (2016), arXiv:1602.03847 [gr-qc].
[17] B. P. Abbott *et al.* (LIGO Scientific, Virgo), Phys. Rev. Lett. **120**, 091101 (2018), arXiv:1710.05837 [gr-qc].
[18] R. Abbott *et al.* (KAGRA, VIRGO, LIGO Scientific), Phys. Rev. X **13**, 011048 (2023), arXiv:2111.03634 [astro-ph.HE].
[19] A. G. Abac *et al.* (LIGO Scientific, VIRGO, KAGRA), arXiv (2025), arXiv:2508.20721 [gr-qc].
[20] M. Maggiore, (1998), arXiv:gr-qc/9803028.
[21] M. Maggiore, Phys. Rept. **331**, 283 (2000), arXiv:gr-qc/9909001.
[22] P. D. Lasky *et al.*, Phys. Rev. X **6**, 011035 (2016), arXiv:1511.05994 [astro-ph.CO].
[23] C. Caprini and D. G. Figueroa, Class. Quant. Grav. **35**, 163001 (2018), arXiv:1801.04268 [astro-ph.CO].
[24] S. Kuroyanagi, T. Chiba, and T. Takahashi, JCAP **11**, 038 (2018), arXiv:1807.00786 [astro-ph.CO].
[25] B. P. Abbott *et al.* (LIGO Scientific, Virgo), Class. Quant. Grav. **33**, 134001 (2016), arXiv:1602.03844 [gr-qc].
[26] D. Davis *et al.* (LIGO), Class. Quant. Grav. **38**, 135014 (2021), arXiv:2101.11673 [astro-ph.IM].
[27] S. Soni *et al.* (LIGO), Class. Quant. Grav. **42**, 085016 (2025), arXiv:2409.02831 [astro-ph.IM].
[28] E. Capote *et al.*, Phys. Rev. D **111**, 062002 (2025), arXiv:2411.14607 [gr-qc].
[29] F. Acernese *et al.* (Virgo), Class. Quant. Grav. **40**, 185006 (2023), arXiv:2210.15633 [gr-qc].
[30] E. Witten, Phys. Rev. D **30**, 272 (1984).
[31] A. Mazumdar and G. White, Rept. Prog. Phys. **82**, 076901 (2019), arXiv:1811.01948 [hep-ph].
[32] M. B. Hindmarsh, M. Lüben, J. Lumma, and M. Pauly, SciPost Phys. Lect. Notes **24**, 1 (2021), arXiv:2008.09136 [astro-ph.CO].
[33] C. Caprini, O. Pujolàs, H. Quelquejay-Leclere, F. Rompineve, and D. A. Steer, Class. Quant. Grav. **42**, 045015 (2025), arXiv:2406.02359 [astro-ph.CO].
[34] R. Jeannerot, J. Rocher, and M. Sakellariadou, Phys. Rev. D **68**, 103514 (2003), arXiv:hep-ph/0308134.
[35] T. W. B. Kibble, J. Phys. A **9**, 1387 (1976).
[36] Y. B. Zeldovich, I. Y. Kobzarev, and L. B. Okun, Zh. Eksp. Teor. Fiz. **67**, 3 (1974).
[37] B. S. Ryden, W. H. Press, and D. N. Spergel, Astrophys. J. **357**, 293 (1990).
[38] M. Hindmarsh, Phys. Rev. Lett. **77**, 4495 (1996), arXiv:hep-ph/9605332.
[39] T. Garagounis and M. Hindmarsh, Phys. Rev. D **68**, 103506 (2003), arXiv:hep-ph/0212359.
[40] J. C. R. E. Oliveira, C. J. A. P. Martins, and P. P. Avelino, Phys. Rev. D **71**, 083509 (2005), arXiv:hep-ph/0410356.
[41] P. P. Avelino, J. C. R. E. Oliveira, and C. J. A. P. Martins, Phys. Lett. B **610**, 1 (2005), arXiv:hep-th/0503226.
[42] A. M. M. Leite and C. J. A. P. Martins, Phys. Rev. D **84**, 103523 (2011), arXiv:1110.3486 [hep-ph].
[43] P. J. E. Peebles and A. Vilenkin, Phys. Rev. D **59**,

063505 (1999), arXiv:astro-ph/9810509.
[44] M. Giovannini, Phys. Rev. D **58**, 083504 (1998), arXiv:hep-ph/9806329.
[45] L. A. Boyle and P. J. Steinhardt, Phys. Rev. D **77**, 063504 (2008), arXiv:astro-ph/0512014.
[46] L. A. Boyle and A. Buonanno, Phys. Rev. **D78**, 043531 (2008), arXiv:0708.2279 [astro-ph].
[47] S. Kuroyanagi, K. Nakayama, and S. Saito, Phys. Rev. D **84**, 123513 (2011), arXiv:1110.4169 [astro-ph.CO].
[48] B. Li, T. Rindler-Daller, and P. R. Shapiro, Phys. Rev. D **89**, 083536 (2014), arXiv:1310.6061 [astro-ph.CO].
[49] B. Li, P. R. Shapiro, and T. Rindler-Daller, Phys. Rev. D **96**, 063505 (2017), arXiv:1611.07961 [astro-ph.CO].
[50] D. G. Figueroa and E. H. Tanin, JCAP **08**, 011 (2019), arXiv:1905.11960 [astro-ph.CO].
[51] B. Li and P. R. Shapiro, JCAP **10**, 024 (2021), arXiv:2107.12229 [astro-ph.CO].
[52] S. Kuroyanagi, T. Takahashi, and S. Yokoyama, JCAP **02**, 003 (2015), arXiv:1407.4785 [astro-ph.CO].
[53] H. Duval, S. Kuroyanagi, A. Mariotti, A. Romero-Rodríguez, and M. Sakellariadou, Phys. Rev. D **110**, 103503 (2024), arXiv:2405.10201 [gr-qc].
[54] M. M. Anber and L. Sorbo, Phys. Rev. D **81**, 043534 (2010), arXiv:0908.4089 [hep-th].
[55] J. L. Cook and L. Sorbo, Phys. Rev. D **85**, 023534 (2012), [Erratum: Phys.Rev.D 86, 069901 (2012)], arXiv:1109.0022 [astro-ph.CO].
[56] E. Dimastrogiovanni and M. Peloso, Phys. Rev. D **87**, 103501 (2013), arXiv:1212.5184 [astro-ph.CO].
[57] T. Fujita, K. Mukaida, K. Murai, and H. Nakatsuka, Phys. Rev. D **105**, 103519 (2022), arXiv:2110.03228 [hep-ph].
[58] G. Domènech, Universe **7**, 398 (2021), arXiv:2109.01398 [gr-qc].
[59] K. Tomita, Prog. Theor. Phys. **37**, 831 (1967).
[60] S. Matarrese, O. Pantano, and D. Saez, Phys. Rev. Lett. **72**, 320 (1994), arXiv:astro-ph/9310036.
[61] S. Matarrese, S. Mollerach, and M. Bruni, Phys. Rev. D **58**, 043504 (1998), arXiv:astro-ph/9707278.
[62] K. N. Ananda, C. Clarkson, and D. Wands, Phys. Rev. D **75**, 123518 (2007), arXiv:gr-qc/0612013.
[63] D. Baumann, P. J. Steinhardt, K. Takahashi, and K. Ichiki, Phys. Rev. D **76**, 084019 (2007), arXiv:hep-th/0703290.
[64] B. Carr and F. Kuhnel, SciPost Phys. Lect. Notes **48**, 1 (2022), arXiv:2110.02821 [astro-ph.CO].
[65] N. Seto and A. Taruya, Phys. Rev. Lett. **99**, 121101 (2007), arXiv:0707.0535 [astro-ph].
[66] P. A. R. Ade *et al.* (Planck), Astron. Astrophys. **594**, A13 (2016), arXiv:1502.01589 [astro-ph.CO].
[67] A. J. Farmer and E. S. Phinney, Monthly Notices of the Royal Astronomical Society **346**, 1197 (2003), https://academic.oup.com/mnras/article-pdf/346/4/1197/18649605/346-4-1197.pdf.
[68] R. Abbott *et al.* (KAGRA, Virgo, LIGO Scientific), Phys. Rev. D **104**, 022004 (2021), arXiv:2101.12130 [gr-qc].
[69] T. Callister, A. S. Biscoveanu, N. Christensen, M. Isi, A. Matas, O. Minazzoli, T. Regimbau, M. Sakellariadou, J. Tasson, and E. Thrane, Phys. Rev. X **7**, 041058 (2017), arXiv:1704.08373 [gr-qc].
[70] B. P. Abbott *et al.* (LIGO Scientific, Virgo), Phys. Rev. Lett. **120**, 201102 (2018), arXiv:1802.10194 [gr-qc].
[71] A. G. Abac *et al.* (LIGO Scientific, VIRGO, KAGRA), arXiv (2025), arXiv:2510.17487 [gr-qc].
[72] N. Christensen and R. Meyer, Rev. Mod. Phys. **94**, 025001 (2022), arXiv:2204.04449 [gr-qc].
[73] V. Mandic, E. Thrane, S. Giampanis, and T. Regimbau, Phys. Rev. Lett. **109**, 171102 (2012).
[74] E. Thrane, N. Christensen, and R. Schofield, Phys. Rev. D **87**, 123009 (2013), arXiv:1303.2613 [astro-ph.IM].
[75] P. M. Meyers, K. Martinovic, N. Christensen, and M. Sakellariadou, Phys. Rev. D **102**, 102005 (2020), arXiv:2008.00789 [gr-qc].
[76] N. Christensen, Phys. Rev. D **46**, 5250 (1992).
[77] N. Christensen, Phys. Rev. D **55**, 448 (1997).
[78] A. Kosowsky, M. S. Turner, and R. Watkins, Phys. Rev. D **45**, 4514 (1992).
[79] A. Kosowsky and M. S. Turner, Phys. Rev. D **47**, 4372 (1993), arXiv:astro-ph/9211004.
[80] M. Hindmarsh, S. J. Huber, K. Rummukainen, and D. J. Weir, Phys. Rev. Lett. **112**, 041301 (2014), arXiv:1304.2433 [hep-ph].
[81] M. Hindmarsh, S. J. Huber, K. Rummukainen, and D. J. Weir, Phys. Rev. D **92**, 123009 (2015), arXiv:1504.03291 [astro-ph.CO].
[82] M. Kamionkowski, A. Kosowsky, and M. S. Turner, Phys. Rev. D **49**, 2837 (1994), arXiv:astro-ph/9310044.
[83] C. Grojean and G. Servant, Phys. Rev. D **75**, 043507 (2007), arXiv:hep-ph/0607107.
[84] V. Vaskonen, Phys. Rev. D **95**, 123515 (2017), arXiv:1611.02073 [hep-ph].
[85] G. C. Dorsch, S. J. Huber, T. Konstandin, and J. M. No, JCAP **05**, 052 (2017), arXiv:1611.05874 [hep-ph].
[86] P. Schwaller, Phys. Rev. Lett. **115**, 181101 (2015), arXiv:1504.07263 [hep-ph].
[87] J. Jaeckel, V. V. Khoze, and M. Spannowsky, Phys. Rev. D **94**, 103519 (2016), arXiv:1602.03901 [hep-ph].
[88] M. Breitbach, J. Kopp, E. Madge, T. Opferkuch, and P. Schwaller, JCAP **07**, 007 (2019), arXiv:1811.11175 [hep-ph].
[89] P. S. B. Dev, F. Ferrer, Y. Zhang, and Y. Zhang, JCAP **11**, 006 (2019), arXiv:1905.00891 [hep-ph].
[90] L. Delle Rose, G. Panico, M. Redi, and A. Tesi, JHEP **04**, 025 (2020), arXiv:1912.06139 [hep-ph].
[91] B. Von Harling, A. Pomarol, O. Pujolas, and F. Rompineve, JHEP **04**, 195 (2020), arXiv:1912.07587 [hep-ph].
[92] D. Croon, T. E. Gonzalo, and G. White, JHEP **02**, 083 (2019), arXiv:1812.02747 [hep-ph].
[93] W.-C. Huang, F. Sannino, and Z.-W. Wang, Phys. Rev. D **102**, 095025 (2020), arXiv:2004.02332 [hep-ph].
[94] S. J. Huber and T. Konstandin, JCAP **05**, 017 (2008), arXiv:0709.2091 [hep-ph].
[95] S. V. Demidov, D. S. Gorbunov, and D. V. Kirpichnikov, Phys. Lett. B **779**, 191 (2018), arXiv:1712.00087 [hep-ph].
[96] N. Craig, N. Levi, A. Mariotti, and D. Redigolo, JHEP **21**, 184 (2020), arXiv:2011.13949 [hep-ph].
[97] L. Randall and G. Servant, JHEP **05**, 054 (2007), arXiv:hep-ph/0607158.
[98] A. Romero, K. Martinovic, T. A. Callister, H.-K. Guo, M. Martínez, M. Sakellariadou, F.-W. Yang, and Y. Zhao, Phys. Rev. Lett. **126**, 151301 (2021), arXiv:2102.01714 [hep-ph].
[99] J. Ellis, M. Lewicki, J. M. No, and V. Vaskonen, JCAP **06**, 024 (2019), arXiv:1903.09642 [hep-ph].
[100] J. Ellis, M. Lewicki, and V. Vaskonen, JCAP **11**, 020

(2020), arXiv:2007.15586 [astro-ph.CO].
[101] C. Badger *et al.*, Phys. Rev. D **107**, 023511 (2023), arXiv:2209.14707 [hep-ph].
[102] M. Hindmarsh, S. J. Huber, K. Rummukainen, and D. J. Weir, Phys. Rev. D **96**, 103520 (2017), [Erratum: Phys.Rev.D 101, 089902 (2020)], arXiv:1704.05871 [astro-ph.CO].
[103] M. Hindmarsh, Phys. Rev. Lett. **120**, 071301 (2018), arXiv:1608.04735 [astro-ph.CO].
[104] M. Hindmarsh and M. Hijazi, JCAP **12**, 062 (2019), arXiv:1909.10040 [astro-ph.CO].
[105] H.-K. Guo, K. Sinha, D. Vagie, and G. White, JCAP **01**, 001 (2021), arXiv:2007.08537 [hep-ph].
[106] D. Cutting, M. Hindmarsh, and D. J. Weir, Phys. Rev. Lett. **125**, 021302 (2020), arXiv:1906.00480 [hep-ph].
[107] C. Caprini *et al.*, JCAP **04**, 001 (2016), arXiv:1512.06239 [astro-ph.CO].
[108] J. R. Espinosa, T. Konstandin, J. M. No, and G. Servant, JCAP **06**, 028 (2010), arXiv:1004.4187 [hep-ph].
[109] J. Ellis, M. Lewicki, and J. M. No, JCAP **07**, 050 (2020), arXiv:2003.07360 [hep-ph].
[110] A. Kosowsky, M. S. Turner, and R. Watkins, Phys. Rev. Lett. **69**, 2026 (1992).
[111] R. Jinno and M. Takimoto, Phys. Rev. D **95**, 024009 (2017), arXiv:1605.01403 [astro-ph.CO].
[112] S. J. Huber and T. Konstandin, JCAP **09**, 022 (2008), arXiv:0806.1828 [hep-ph].
[113] D. Cutting, M. Hindmarsh, and D. J. Weir, Phys. Rev. D **97**, 123513 (2018), arXiv:1802.05712 [astro-ph.CO].
[114] D. Cutting, E. G. Escartin, M. Hindmarsh, and D. J. Weir, Phys. Rev. D **103**, 023531 (2021), arXiv:2005.13537 [astro-ph.CO].
[115] M. Lewicki and V. Vaskonen, Eur. Phys. J. C **80**, 1003 (2020), arXiv:2007.04967 [astro-ph.CO].
[116] M. Lewicki and V. Vaskonen, Eur. Phys. J. C **81**, 437 (2021), [Erratum: Eur.Phys.J.C 81, 1077 (2021)], arXiv:2012.07826 [astro-ph.CO].
[117] Y. Di, J. Wang, R. Zhou, L. Bian, R.-G. Cai, and J. Liu, Phys. Rev. Lett. **126**, 251102 (2021), arXiv:2012.15625 [astro-ph.CO].
[118] H.-k. Guo, F. Hajkarim, K. Sinha, G. White, and Y. Xiao, JCAP **02**, 056 (2025), arXiv:2407.02580 [hep-ph].
[119] A. I. Renzini *et al.*, Astrophys. J. **952**, 25 (2023), arXiv:2303.15696 [gr-qc].
[120] K. Enqvist, J. Ignatius, K. Kajantie, and K. Rummukainen, Phys. Rev. D **45**, 3415 (1992).
[121] R.-G. Cai and S.-J. Wang, Sci. China Phys. Mech. Astron. **61**, 080411 (2018), arXiv:1803.03002 [gr-qc].
[122] L. Giombi and M. Hindmarsh, JCAP **03**, 059 (2024), arXiv:2307.12080 [astro-ph.CO].
[123] R. Jinno and J. Kume, JCAP **02**, 057 (2025), arXiv:2408.10770 [gr-qc].
[124] T. W. B. Kibble, Phys. Rept. **67**, 183 (1980).
[125] W. H. Zurek, Nature **317**, 505 (1985).
[126] W. H. Zurek, Phys. Rept. **276**, 177 (1996), arXiv:cond-mat/9607135.
[127] S. Weinberg, Phys. Rev. Lett. **40**, 223 (1978).
[128] F. Wilczek, Phys. Rev. Lett. **40**, 279 (1978).
[129] M. A. Shifman, A. I. Vainshtein, and V. I. Zakharov, Nucl. Phys. **B166**, 493 (1980).
[130] J. E. Kim, Phys. Rev. Lett. **43**, 103 (1979).
[131] A. R. Zhitnitsky, Sov. J. Nucl. Phys. **31**, 260 (1980), [Yad. Fiz.31,497(1980)].
[132] M. Dine, W. Fischler, and M. Srednicki, Phys. Lett. **104B**, 199 (1981).
[133] J. Preskill, M. B. Wise, and F. Wilczek, Phys. Lett. B **120**, 127 (1983).
[134] L. F. Abbott and P. Sikivie, Phys. Lett. **120B**, 133 (1983).
[135] M. Dine and W. Fischler, Phys. Lett. **120B**, 137 (1983).
[136] X. Niu, W. Xue, and F. Yang, JHEP **02**, 093 (2024), arXiv:2311.07639 [hep-ph].
[137] B. P. Abbott *et al.* (LIGO Scientific, Virgo), Phys. Rev. D **97**, 102002 (2018), arXiv:1712.01168 [gr-qc].
[138] B. P. Abbott *et al.* (LIGO Scientific, Virgo), Phys. Rev. D **100**, 061101 (2019), arXiv:1903.02886 [gr-qc].
[139] R. Abbott *et al.* (LIGO Scientific, Virgo, KAGRA), Phys. Rev. Lett. **126**, 241102 (2021), arXiv:2101.12248 [gr-qc].
[140] A. Afzal *et al.* (NANOGrav), Astrophys. J. Lett. **951**, L11 (2023), arXiv:2306.16219 [astro-ph.HE].
[141] J. Antoniadis *et al.* (EPTA, InPTA), Astron. Astrophys. **685**, A94 (2024), arXiv:2306.16227 [astro-ph.CO].
[142] N. Yonemaru *et al.*, Mon. Not. Roy. Astron. Soc. **501**, 701 (2021), arXiv:2011.13490 [gr-qc].
[143] P. Auclair *et al.*, JCAP **04**, 034 (2020), arXiv:1909.00819 [astro-ph.CO].
[144] P. Auclair *et al.* (LISA Cosmology Working Group), Living Rev. Rel. **26**, 5 (2023), arXiv:2204.05434 [astro-ph.CO].
[145] Z.-C. Chen, Q.-G. Huang, C. Liu, L. Liu, X.-J. Liu, Y. Wu, Y.-M. Wu, Z. Yi, and Z.-Q. You, JCAP **03**, 022 (2024), arXiv:2310.00411 [astro-ph.IM].
[146] B. Canuel *et al.*, Class. Quant. Grav. **37**, 225017 (2020), arXiv:1911.03701 [physics.atom-ph].
[147] M. Sakellariadou, Phys. Rev. D **42**, 354 (1990), [Erratum: Phys. Rev. D 43, 4150 (1991)].
[148] M. Sakellariadou, Phys. Rev. D **44**, 3767 (1991).
[149] J. J. Blanco-Pillado, K. D. Olum, and B. Shlaer, Phys. Rev. D **89**, 023512 (2014), arXiv:1309.6637 [astro-ph.CO].
[150] L. Lorenz, C. Ringeval, and M. Sakellariadou, JCAP **10**, 003 (2010), arXiv:1006.0931 [astro-ph.CO].
[151] C. Ringeval, M. Sakellariadou, and F. Bouchet, JCAP **02**, 023 (2007), arXiv:astro-ph/0511646.
[152] P. Auclair, C. Ringeval, M. Sakellariadou, and D. Steer, JCAP **06**, 015 (2019), arXiv:1903.06685 [astro-ph.CO].
[153] M. Hindmarsh, Phys. Lett. B **251**, 28 (1990).
[154] D. G. Figueroa, M. Hindmarsh, and J. Urrestilla, Phys. Rev. Lett. **110**, 101302 (2013), arXiv:1212.5458 [astro-ph.CO].
[155] D. Camargo Neves da Cunha, C. Ringeval, and F. R. Bouchet, JCAP **09**, 078 (2022), arXiv:2205.04349 [astro-ph.CO].
[156] M. Hindmarsh, S. Stuckey, and N. Bevis, Phys. Rev. D **79**, 123504 (2009), arXiv:0812.1929 [hep-th].
[157] D. Matsunami, L. Pogosian, A. Saurabh, and T. Vachaspati, Phys. Rev. Lett. **122**, 201301 (2019), arXiv:1903.05102 [hep-ph].
[158] M. Hindmarsh, J. Lizarraga, A. Urio, and J. Urrestilla, Phys. Rev. D **104**, 043519 (2021), arXiv:2103.16248 [astro-ph.CO].
[159] J. Baeza-Ballesteros, E. J. Copeland, D. G. Figueroa, and J. Lizarraga, Phys. Rev. D **112**, 043540 (2025), arXiv:2408.02364 [astro-ph.CO].
[160] M. Kawasaki, K. Miyamoto, and K. Nakayama, Phys. Rev. D **81**, 103523 (2010), arXiv:1002.0652 [astro-

ph.CO].
[161] Y. Matsui, K. Horiguchi, D. Nitta, and S. Kuroyanagi, JCAP **11**, 005 (2016), arXiv:1605.08768 [astro-ph.CO].
[162] Y. Matsui and S. Kuroyanagi, Phys. Rev. D **100**, 123515 (2019), arXiv:1902.09120 [astro-ph.CO].
[163] E. J. Copeland and T. W. B. Kibble, Phys. Rev. D **80**, 123523 (2009), arXiv:0909.1960 [astro-ph.CO].
[164] R. D. Peccei and H. R. Quinn, Phys. Rev. Lett. **38**, 1440 (1977).
[165] A. Vilenkin and A. E. Everett, Phys. Rev. Lett. **48**, 1867 (1982).
[166] P. Sikivie, Phys. Rev. Lett. **48**, 1156 (1982).
[167] R. Z. Ferreira, A. Notari, O. Pujolas, and F. Rompineve, Phys. Rev. Lett. **128**, 141101 (2022), arXiv:2107.07542 [hep-ph].
[168] R. Z. Ferreira, A. Notari, O. Pujolas, and F. Rompineve, JCAP **02**, 001 (2023), arXiv:2204.04228 [astro-ph.CO].
[169] Y. Jiang and Q.-G. Huang, Phys. Rev. D **106**, 103036 (2022), arXiv:2208.00697 [astro-ph.CO].
[170] B. Holdom and M. E. Peskin, Nucl. Phys. B **208**, 397 (1982).
[171] B. Holdom, Phys. Lett. B **154**, 316 (1985), [Erratum: Phys.Lett.B 156, 452 (1985)].
[172] J. M. Flynn and L. Randall, Nucl. Phys. B **293**, 731 (1987).
[173] V. A. Rubakov, JETP Lett. **65**, 621 (1997), arXiv:hep-ph/9703409.
[174] Z. Berezhiani, L. Gianfagna, and M. Giannotti, Phys. Lett. B **500**, 286 (2001), arXiv:hep-ph/0009290.
[175] K. Choi and H. D. Kim, Phys. Rev. D **59**, 072001 (1999), arXiv:hep-ph/9809286.
[176] S. Blasi, A. Mariotti, A. Rase, A. Sevrin, and K. Turbang, JCAP **04**, 008 (2023), arXiv:2210.14246 [hep-ph].
[177] G. B. Gelmini, S. Pascoli, E. Vitagliano, and Y.-L. Zhou, JCAP **02**, 032 (2021), arXiv:2009.01903 [hep-ph].
[178] S. Mishra and U. A. Yajnik, Phys. Rev. D **81**, 045010 (2010), arXiv:0911.1578 [hep-ph].
[179] E. Witten, Nucl. Phys. B **202**, 253 (1982).
[180] J. R. Ellis, K. Enqvist, D. V. Nanopoulos, K. A. Olive, M. Quiros, and F. Zwirner, Phys. Lett. B **176**, 403 (1986).
[181] S. A. Abel, S. Sarkar, and P. L. White, Nucl. Phys. B **454**, 663 (1995), arXiv:hep-ph/9506359.
[182] G. R. Dvali and M. A. Shifman, Phys. Lett. B **396**, 64 (1997), [Erratum: Phys.Lett.B 407, 452 (1997)], arXiv:hep-th/9612128.
[183] A. Kovner, M. A. Shifman, and A. V. Smilga, Phys. Rev. D **56**, 7978 (1997), arXiv:hep-th/9706089.
[184] G. Lazarides, Q. Shafi, and T. F. Walsh, Nucl. Phys. B **195**, 157 (1982).
[185] A. E. Everett and A. Vilenkin, Nucl. Phys. B **207**, 43 (1982).
[186] G. Lazarides and Q. Shafi, Phys. Lett. B **115**, 21 (1982).
[187] N. Craig, I. Garcia Garcia, G. Koszegi, and A. McCune, JHEP **09**, 130 (2021), arXiv:2012.13416 [hep-ph].
[188] G. B. Gelmini, M. Gleiser, and E. W. Kolb, Phys. Rev. D **39**, 1558 (1989).
[189] T. Banks and L. J. Dixon, Nucl. Phys. B **307**, 93 (1988).
[190] M. Kamionkowski and J. March-Russell, Phys. Lett. B **282**, 137 (1992), arXiv:hep-th/9202003.
[191] T. Banks and N. Seiberg, Phys. Rev. D **83**, 084019 (2011), arXiv:1011.5120 [hep-th].
[192] D. Harlow and H. Ooguri, Commun. Math. Phys. **383**, 1669 (2021), arXiv:1810.05338 [hep-th].
[193] K. Saikawa, Universe **3**, 40 (2017), arXiv:1703.02576 [hep-ph].
[194] T. Hiramatsu, M. Kawasaki, and K. Saikawa, JCAP **05**, 032 (2010), arXiv:1002.1555 [astro-ph.CO].
[195] T. Hiramatsu, M. Kawasaki, K. Saikawa, and T. Sekiguchi, JCAP **01**, 001 (2013), arXiv:1207.3166 [hep-ph].
[196] T. Hiramatsu, M. Kawasaki, and K. Saikawa, JCAP **02**, 031 (2014), arXiv:1309.5001 [astro-ph.CO].
[197] N. Kitajima, J. Lee, K. Murai, F. Takahashi, and W. Yin, Phys. Lett. B **851**, 138586 (2024), arXiv:2306.17146 [hep-ph].
[198] R. Z. Ferreira, A. Notari, O. Pujolàs, and F. Rompineve, JCAP **06**, 020 (2024), arXiv:2401.14331 [astro-ph.CO].
[199] L. Barsotti, L. McCuller, M. Evans, and P. Fritschel, LIGO Document T1800042-v5 (2020).
[200] N. Seto and J. Yokoyama, J. Phys. Soc. Jap. **72**, 3082 (2003), arXiv:gr-qc/0305096.
[201] T. L. Smith, M. Kamionkowski, and A. Cooray, Phys. Rev. D **73**, 023504 (2006), arXiv:astro-ph/0506422.
[202] K. Nakayama, S. Saito, Y. Suwa, and J. Yokoyama, Phys. Rev. D **77**, 124001 (2008), arXiv:0802.2452 [hep-ph].
[203] K. Nakayama, S. Saito, Y. Suwa, and J. Yokoyama, JCAP **06**, 020 (2008), arXiv:0804.1827 [astro-ph].
[204] K. Nakayama and J. Yokoyama, JCAP **01**, 010 (2010), arXiv:0910.0715 [astro-ph.CO].
[205] S. Kuroyanagi, C. Ringeval, and T. Takahashi, Phys. Rev. D **87**, 083502 (2013), arXiv:1301.1778 [astro-ph.CO].
[206] N. Bernal and F. Hajkarim, Phys. Rev. D **100**, 063502 (2019), arXiv:1905.10410 [astro-ph.CO].
[207] N. Bernal, A. Ghoshal, F. Hajkarim, and G. Lambiase, JCAP **11**, 051 (2020), arXiv:2008.04959 [gr-qc].
[208] M. R. Haque, D. Maity, T. Paul, and L. Sriramkumar, Phys. Rev. D **104**, 063513 (2021), arXiv:2105.09242 [astro-ph.CO].
[209] S. S. Mishra, V. Sahni, and A. A. Starobinsky, JCAP **05**, 075 (2021), arXiv:2101.00271 [gr-qc].
[210] A. Chakraborty, M. R. Haque, D. Maity, and R. Mondal, Phys. Rev. D **108**, 023515 (2023), arXiv:2304.13637 [astro-ph.CO].
[211] M. S. Turner, Phys. Rev. D **28**, 1243 (1983).
[212] R. T. Co, D. Dunsky, N. Fernandez, A. Ghalsasi, L. J. Hall, K. Harigaya, and J. Shelton, JHEP **09**, 116 (2022), arXiv:2108.09299 [hep-ph].
[213] R. T. Co and K. Harigaya, Phys. Rev. Lett. **124**, 111602 (2020), arXiv:1910.02080 [hep-ph].
[214] Y. Gouttenoire, G. Servant, and P. Simakachorn, arXiv (2021), arXiv:2111.01150 [hep-ph].
[215] Y. Gouttenoire, G. Servant, and P. Simakachorn, arXiv (2021), arXiv:2108.10328 [hep-ph].
[216] T. J. Battefeld and D. A. Easson, Phys. Rev. D **70**, 103516 (2004), arXiv:hep-th/0408154.
[217] F. Apers, J. P. Conlon, M. Mosny, and F. Revello, JHEP **08**, 156 (2023), arXiv:2212.10293 [hep-th].
[218] H. M. Lee, A. G. Menkara, M.-J. Seong, and J.-H. Song, JHEP **05**, 295 (2024), arXiv:2310.17710 [hep-ph].
[219] K. Harigaya, K. Inomata, and T. Terada, Phys. Rev. D **108**, L081303 (2023), arXiv:2305.14242 [hep-ph].
[220] K. Harigaya, K. Inomata, and T. Terada, Phys. Rev. D **108**, 123538 (2023), arXiv:2309.00228 [astro-ph.CO].

[221] C. Eröncel, Y. Gouttenoire, R. Sato, G. Servant, and P. Simakachorn, Phys. Rev. Lett. **135**, 101002 (2025), arXiv:2501.17226 [hep-ph].

[222] P. A. R. Ade *et al.* (BICEP, Keck), Phys. Rev. Lett. **127**, 151301 (2021), arXiv:2110.00483 [astro-ph.CO].

[223] E. Allys *et al.* (LiteBIRD), PTEP **2023**, 042F01 (2023), arXiv:2202.02773 [astro-ph.IM].

[224] T.-H. Yeh, J. Shelton, K. A. Olive, and B. D. Fields, JCAP **10**, 046 (2022), arXiv:2207.13133 [astro-ph.CO].

[225] N. Barnaby, E. Pajer, and M. Peloso, Phys. Rev. D **85**, 023525 (2012), arXiv:1110.3327 [astro-ph.CO].

[226] N. Barnaby, R. Namba, and M. Peloso, JCAP **04**, 009 (2011), arXiv:1102.4333 [astro-ph.CO].

[227] N. Barnaby and M. Peloso, Phys. Rev. Lett. **106**, 181301 (2011), arXiv:1011.1500 [hep-ph].

[228] P. D. Meerburg and E. Pajer, JCAP **02**, 017 (2013), arXiv:1203.6076 [astro-ph.CO].

[229] V. Domcke, F. Muia, M. Pieroni, and L. T. Witkowski, JCAP **07**, 048 (2017), arXiv:1704.03464 [astro-ph.CO].

[230] J. Garcia-Bellido, M. Peloso, and C. Unal, JCAP **12**, 031 (2016), arXiv:1610.03763 [astro-ph.CO].

[231] V. Domcke, M. Pieroni, and P. Binétruy, JCAP **06**, 031 (2016), arXiv:1603.01287 [astro-ph.CO].

[232] E. Dimastrogiovanni, M. Fasiello, and T. Fujita, JCAP **01**, 019 (2017), arXiv:1608.04216 [astro-ph.CO].

[233] J. Garcia-Bellido, A. Papageorgiou, M. Peloso, and L. Sorbo, JCAP **01**, 034 (2024), arXiv:2303.13425 [astro-ph.CO].

[234] J. Garcia-Bellido, M. Peloso, and C. Unal, JCAP **09**, 013 (2017), arXiv:1707.02441 [astro-ph.CO].

[235] A. Maleknejad, JHEP **07**, 104 (2016), arXiv:1604.03327 [hep-ph].

[236] B. Thorne, T. Fujita, M. Hazumi, N. Katayama, E. Komatsu, and M. Shiraishi, Phys. Rev. D **97**, 043506 (2018), arXiv:1707.03240 [astro-ph.CO].

[237] P. Adshead, E. Martinec, and M. Wyman, Phys. Rev. D **88**, 021302 (2013), arXiv:1301.2598 [hep-th].

[238] P. Adshead, E. Martinec, and M. Wyman, JHEP **09**, 087 (2013), arXiv:1305.2930 [hep-th].

[239] I. Obata and J. Soda, Phys. Rev. D **94**, 044062 (2016), arXiv:1607.01847 [astro-ph.CO].

[240] R. R. Caldwell and C. Devulder, Phys. Rev. D **97**, 023532 (2018), arXiv:1706.03765 [astro-ph.CO].

[241] G. Dall'Agata, Phys. Lett. B **782**, 139 (2018), arXiv:1804.03104 [hep-th].

[242] E. McDonough and S. Alexander, JCAP **11**, 030 (2018), arXiv:1806.05684 [hep-th].

[243] P. Adshead, E. Martinec, E. I. Sfakianakis, and M. Wyman, JHEP **12**, 137 (2016), arXiv:1609.04025 [hep-th].

[244] I. Obata, T. Miura, and J. Soda, Phys. Rev. D **92**, 063516 (2015), [Addendum: Phys.Rev.D 95, 109902 (2017)], arXiv:1412.7620 [hep-ph].

[245] I. Obata and J. Soda, Phys. Rev. D **93**, 123502 (2016), [Addendum: Phys.Rev.D 95, 109903 (2017)], arXiv:1602.06024 [hep-th].

[246] V. Domcke, B. Mares, F. Muia, and M. Pieroni, JCAP **04**, 034 (2019), arXiv:1807.03358 [hep-ph].

[247] T. Fujita, K. Imagawa, and K. Murai, JCAP **07**, 046 (2022), arXiv:2203.15273 [astro-ph.CO].

[248] P. Adshead and M. Wyman, Phys. Rev. Lett. **108**, 261302 (2012), arXiv:1202.2366 [hep-th].

[249] E. Dimastrogiovanni, M. Fasiello, and A. J. Tolley, JCAP **02**, 046 (2013), arXiv:1211.1396 [hep-th].

[250] A. Maleknejad and E. Erfani, JCAP **03**, 016 (2014), arXiv:1311.3361 [hep-th].

[251] I. Wolfson, A. Maleknejad, T. Murata, E. Komatsu, and T. Kobayashi, JCAP **09**, 031 (2021), arXiv:2105.06259 [gr-qc].

[252] T. Murata, T. Fujita, and T. Kobayashi, Phys. Rev. D **107**, 043508 (2023), arXiv:2211.09489 [gr-qc].

[253] A. A. Starobinsky, JETP Lett. **55**, 489 (1992).

[254] J. Martin and L. Sriramkumar, JCAP **01**, 008 (2012), arXiv:1109.5838 [astro-ph.CO].

[255] C. Badger, H. Duval, T. Fujita, S. Kuroyanagi, A. Romero-Rodríguez, and M. Sakellariadou, Phys. Rev. D **110**, 084063 (2024), arXiv:2406.11742 [astro-ph.CO].

[256] B. J. Carr, K. Kohri, Y. Sendouda, and J. Yokoyama, Phys. Rev. D **81**, 104019 (2010), arXiv:0912.5297 [astro-ph.CO].

[257] B. Carr, K. Kohri, Y. Sendouda, and J. Yokoyama, Rept. Prog. Phys. **84**, 116902 (2021), arXiv:2002.12778 [astro-ph.CO].

[258] A. Caravano, E. Komatsu, K. D. Lozanov, and J. Weller, Phys. Rev. D **108**, 043504 (2023), arXiv:2204.12874 [astro-ph.CO].

[259] A. Papageorgiou, M. Peloso, and C. Unal, JCAP **07**, 004 (2019), arXiv:1904.01488 [astro-ph.CO].

[260] R. Saito and J. Yokoyama, Phys. Rev. Lett. **102**, 161101 (2009), [Erratum: Phys.Rev.Lett. 107, 069901 (2011)], arXiv:0812.4339 [astro-ph].

[261] R. Saito and J. Yokoyama, Prog. Theor. Phys. **123**, 867 (2010), [Erratum: Prog.Theor.Phys. 126, 351–352 (2011)], arXiv:0912.5317 [astro-ph.CO].

[262] B. J. Carr and J. E. Lidsey, Phys. Rev. D **48**, 543 (1993).

[263] B. J. Carr, J. Gilbert, and J. E. Lidsey, Phys. Rev. D **50**, 4853 (1994), arXiv:astro-ph/9405027.

[264] S. J. Kapadia, K. L. Pandey, T. Suyama, and P. Ajith, Phys. Rev. D **101**, 123535 (2020), arXiv:2005.05693 [astro-ph.CO].

[265] S. J. Kapadia, K. Lal Pandey, T. Suyama, S. Kandhasamy, and P. Ajith, Astrophys. J. Lett. **910**, L4 (2021), arXiv:2009.05514 [gr-qc].

[266] A. Romero-Rodriguez, M. Martinez, O. Pujolàs, M. Sakellariadou, and V. Vaskonen, Phys. Rev. Lett. **128**, 051301 (2022), arXiv:2107.11660 [gr-qc].

[267] Y. Jiang, C. Yuan, C.-Z. Li, and Q.-G. Huang, JCAP **12**, 016 (2024), arXiv:2409.07976 [astro-ph.CO].

[268] S. M. Leach, I. J. Grivell, and A. R. Liddle, Phys. Rev. D **62**, 043516 (2000), arXiv:astro-ph/0004296.

[269] L. Alabidi and K. Kohri, Phys. Rev. D **80**, 063511 (2009), arXiv:0906.1398 [astro-ph.CO].

[270] L. Alabidi, K. Kohri, M. Sasaki, and Y. Sendouda, JCAP **09**, 017 (2012), arXiv:1203.4663 [astro-ph.CO].

[271] P. Ivanov, P. Naselsky, and I. Novikov, Phys. Rev. D **50**, 7173 (1994).

[272] J. García-Bellido and E. Ruiz Morales, Phys. Dark Univ. **18**, 47 (2017), arXiv:1702.03901 [astro-ph.CO].

[273] H. Motohashi and W. Hu, Phys. Rev. D **96**, 063503 (2017), arXiv:1706.06784 [astro-ph.CO].

[274] J. Garcia-Bellido, A. D. Linde, and D. Wands, Phys. Rev. D **54**, 6040 (1996), arXiv:astro-ph/9605094.

[275] S. Clesse and J. García-Bellido, Phys. Rev. **D92**, 023524 (2015), arXiv:1501.07565 [astro-ph.CO].

[276] S. Groot Nibbelink and B. J. W. van Tent, Class. Quant. Grav. **19**, 613 (2002), arXiv:hep-ph/0107272.

[277] G. A. Palma, S. Sypsas, and C. Zenteno, Phys.

Rev. Lett. **125**, 121301 (2020), arXiv:2004.06106 [astro-ph.CO].
[278] S. Pi and M. Sasaki, JCAP **09**, 037 (2020), arXiv:2005.12306 [gr-qc].
[279] R.-g. Cai, S. Pi, and M. Sasaki, Phys. Rev. Lett. **122**, 201101 (2019), arXiv:1810.11000 [astro-ph.CO].
[280] C. Unal, Phys. Rev. D **99**, 041301 (2019), arXiv:1811.09151 [astro-ph.CO].
[281] C. Yuan and Q.-G. Huang, Phys. Lett. B **821**, 136606 (2021), arXiv:2007.10686 [astro-ph.CO].
[282] P. Adshead, K. D. Lozanov, and Z. J. Weiner, JCAP **10**, 080 (2021), arXiv:2105.01659 [astro-ph.CO].
[283] K. T. Abe, R. Inui, Y. Tada, and S. Yokoyama, JCAP **05**, 044 (2023), arXiv:2209.13891 [astro-ph.CO].
[284] R. Inui, S. Jaraba, S. Kuroyanagi, and S. Yokoyama, JCAP **05**, 082 (2024), arXiv:2311.05423 [astro-ph.CO].
[285] G. Perna, C. Testini, A. Ricciardone, and S. Matarrese, JCAP **05**, 086 (2024), arXiv:2403.06962 [astro-ph.CO].
[286] J. R. Espinosa, D. Racco, and A. Riotto, JCAP **09**, 012 (2018), arXiv:1804.07732 [hep-ph].
[287] K. Kohri and T. Terada, Phys. Rev. D **97**, 123532 (2018), arXiv:1804.08577 [gr-qc].
[288] G. F. Chapline, Nature **253**, 251 (1975).
[289] A. M. Green and B. J. Kavanagh, J. Phys. G **48**, 043001 (2021), arXiv:2007.10722 [astro-ph.CO].
[290] S. Bird, I. Cholis, J. B. Munoz, Y. Ali-Haimoud, M. Kamionkowski, E. D. Kovetz, A. Raccanelli, and A. G. Riess, Phys. Rev. Lett. **116**, 201301 (2016), arXiv:1603.00464 [astro-ph.CO].
[291] M. Sasaki, T. Suyama, T. Tanaka, and S. Yokoyama, Phys. Rev. Lett. **117**, 061101 (2016), [erratum: Phys. Rev. Lett.121,no.5,059901(2018)], arXiv:1603.08338 [astro-ph.CO].
[292] S. Clesse and J. García-Bellido, Phys. Dark Univ. **15**, 142 (2017), arXiv:1603.05234 [astro-ph.CO].
[293] A. Hall, A. D. Gow, and C. T. Byrnes, Phys. Rev. D **102**, 123524 (2020), arXiv:2008.13704 [astro-ph.CO].
[294] G. Hütsi, M. Raidal, V. Vaskonen, and H. Veermäe, JCAP **03**, 068 (2021), arXiv:2012.02786 [astro-ph.CO].
[295] C. Boehm, A. Kobakhidze, C. A. J. O'hare, Z. S. C. Picker, and M. Sakellariadou, JCAP **03**, 078 (2021), arXiv:2008.10743 [astro-ph.CO].
[296] Z.-C. Chen, C. Yuan, and Q.-G. Huang, Phys. Lett. B **829**, 137040 (2022), arXiv:2108.11740 [astro-ph.CO].
[297] V. De Luca, G. Franciolini, P. Pani, and A. Riotto, JCAP **05**, 003 (2021), arXiv:2102.03809 [astro-ph.CO].
[298] G. Franciolini, V. Baibhav, V. De Luca, K. K. Y. Ng, K. W. K. Wong, E. Berti, P. Pani, A. Riotto, and S. Vitale, Phys. Rev. D **105**, 083526 (2022), arXiv:2105.03349 [gr-qc].
[299] V. Mandic, S. Bird, and I. Cholis, Phys. Rev. Lett. **117**, 201102 (2016), arXiv:1608.06699 [astro-ph.CO].
[300] S. Clesse and J. García-Bellido, Phys. Dark Univ. **18**, 105 (2017), arXiv:1610.08479 [astro-ph.CO].
[301] S. Mukherjee, M. S. P. Meinema, and J. Silk, Mon. Not. Roy. Astron. Soc. **510**, 6218 (2022), arXiv:2107.02181 [astro-ph.CO].
[302] S. Wang, Y.-F. Wang, Q.-G. Huang, and T. G. F. Li, Phys. Rev. Lett. **120**, 191102 (2018), arXiv:1610.08725 [astro-ph.CO].
[303] M. Raidal, V. Vaskonen, and H. Veermäe, JCAP **09**, 037 (2017), arXiv:1707.01480 [astro-ph.CO].
[304] S. Mukherjee and J. Silk, Mon. Not. Roy. Astron. Soc. **506**, 3977 (2021), arXiv:2105.11139 [gr-qc].
[305] E. Bagui and S. Clesse, Phys. Dark Univ. **38**, 101115 (2022), arXiv:2110.07487 [astro-ph.CO].
[306] M. Braglia, J. Garcia-Bellido, and S. Kuroyanagi, JCAP **12**, 012 (2021), arXiv:2110.07488 [astro-ph.CO].
[307] M. Braglia, J. Garcia-Bellido, and S. Kuroyanagi, Mon. Not. Roy. Astron. Soc. **519**, 6008 (2023), arXiv:2201.13414 [astro-ph.CO].
[308] K. Inomata, K. Kohri, and T. Terada, Phys. Rev. D **109**, 063506 (2024), arXiv:2306.17834 [astro-ph.CO].
[309] A. D. Gow, C. T. Byrnes, and A. Hall, Phys. Rev. D **105**, 023503 (2022), arXiv:2009.03204 [astro-ph.CO].
[310] P. Ajith *et al.*, Phys. Rev. Lett. **106**, 241101 (2011), arXiv:0909.2867 [gr-qc].
[311] S. Clesse, J. García-Bellido, and S. Orani, arXiv (2018), arXiv:1812.11011 [astro-ph.CO].
[312] A. Romero-Rodríguez and S. Kuroyanagi, arXiv (2024), arXiv:2407.00205 [astro-ph.CO].
[313] T. Boybeyi, S. Clesse, S. Kuroyanagi, and M. Sakellariadou, Phys. Rev. D **112**, 023551 (2025).
[314] T. Nakamura, M. Sasaki, T. Tanaka, and K. S. Thorne, Astrophys. J. Lett. **487**, L139 (1997), arXiv:astro-ph/9708060.
[315] K. Ioka, T. Chiba, T. Tanaka, and T. Nakamura, Phys. Rev. D **58**, 063003 (1998), arXiv:astro-ph/9807018.
[316] Y. Ali-Haïmoud, E. D. Kovetz, and M. Kamionkowski, Phys. Rev. D **96**, 123523 (2017), arXiv:1709.06576 [astro-ph.CO].
[317] B. Kocsis, T. Suyama, T. Tanaka, and S. Yokoyama, Astrophys. J. **854**, 41 (2018), arXiv:1709.09007 [astro-ph.CO].
[318] M. Raidal, C. Spethmann, V. Vaskonen, and H. Veermäe, arXiv (2018), arXiv:1812.01930 [astro-ph.CO].
[319] G. D. Quinlan and S. L. Shapiro, Astrophys. J. **343**, 725 (1989).
[320] H. Mouri and Y. Taniguchi, Astrophys. J. Lett. **566**, L17 (2002), arXiv:astro-ph/0201102.
[321] S. Clesse and J. Garcia-Bellido, Phys. Dark Univ. **38**, 101111 (2022), arXiv:2007.06481 [astro-ph.CO].
[322] M. Zumalacarregui and U. Seljak, Phys. Rev. Lett. **121**, 141101 (2018), arXiv:1712.02240 [astro-ph.CO].
[323] P. Tisserand *et al.* (EROS-2), Astron. Astrophys. **469**, 387 (2007), arXiv:astro-ph/0607207.
[324] P. Mróz, A. Udalski, M. K. Szymański, I. Soszyński, Ł. Wyrzykowski, P. Pietrukowicz, S. Kozłowski, R. Poleski, J. Skowron, D. Skowron, *et al.*, Nature **632**, 749 (2024).
[325] D. Agius, R. Essig, D. Gaggero, F. Scarcella, G. Suczewski, and M. Valli, JCAP **07**, 003 (2024), arXiv:2403.18895 [hep-ph].
[326] M. Satoh, S. Kanno, and J. Soda, Phys. Rev. D **77**, 023526 (2008).
[327] N. Bartolo, L. Caloni, G. Orlando, and A. Ricciardone, Journal of Cosmology and Astroparticle Physics **2021**, 073 (2021).
[328] T. Takahashi and J. Soda, Phys. Rev. Lett. **102**, 231301 (2009).
[329] N. Bartolo, G. Orlando, and M. Shiraishi, Journal of Cosmology and Astroparticle Physics **2019**, 050 (2019).
[330] W. D. Garretson, G. B. Field, and S. M. Carroll, Phys. Rev. D **46**, 5346 (1992).
[331] M. M. Anber and L. Sorbo, Journal of Cosmology and Astroparticle Physics **2006**, 018 (2006).
[332] N. Barnaby and M. Peloso, Phys. Rev. Lett. **106**,

181301 (2011).
[333] J. L. Cook and L. Sorbo, Phys. Rev. D **85**, 023534 (2012).
[334] L. Sorbo, Journal of Cosmology and Astroparticle Physics **2011**, 003 (2011).
[335] M. M. Anber and L. Sorbo, Phys. Rev. D **85**, 123537 (2012).
[336] M. Kamionkowski, A. Kosowsky, and M. S. Turner, Phys. Rev. D **49**, 2837 (1994).
[337] E. Witten, Phys. Rev. D **30**, 272 (1984).
[338] A. Brandenburg, K. Enqvist, and P. Olesen, Phys. Rev. D **54**, 1291 (1996).
[339] M. Christensson, M. Hindmarsh, and A. Brandenburg, Phys. Rev. E **64**, 056405 (2001).
[340] T. Kahniashvili, A. Brandenburg, A. G. Tevzadze, and B. Ratra, Phys. Rev. D **81**, 123002 (2010).
[341] A. Brandenburg, T. Kahniashvili, S. Mandal, A. Roper Pol, A. G. Tevzadze, and T. Vachaspati, Phys. Rev. Fluids **4**, 024608 (2019).
[342] A. Brandenburg, Y. He, T. Kahniashvili, M. Rheinhardt, and J. Schober, The Astrophysical Journal **911**, 110 (2021).
[343] A. Agrawal, T. Fujita, and E. Komatsu, Phys. Rev. D **97**, 103526 (2018), arXiv:1707.03023 [astro-ph.CO].
[344] S. G. Crowder, R. Namba, V. Mandic, S. Mukohyama, and M. Peloso, Phys. Lett. B **726**, 66 (2013), arXiv:1212.4165 [astro-ph.CO].
[345] T. Kahniashvili, A. Brandenburg, G. Gogoberidze, S. Mandal, and A. Roper Pol, Phys. Rev. Res. **3**, 013193 (2021), arXiv:2011.05556 [astro-ph.CO].
[346] L. Kisslinger and T. Kahniashvili, Phys. Rev. D **92**, 043006 (2015).
[347] M. Lesieur, *Turbulence in Fluids* (Springer Netherlands, 1997).
[348] S. S. Moiseev and O. Chkhetiani, Journal of Experimental and Theoretical Physics **83**, 192 (1996).
[349] A. J. Long, E. Sabancilar, and T. Vachaspati, Journal of Cosmology and Astroparticle Physics **2014**, 036–036 (2014).
[350] G. Dorsch, S. Huber, T. Konstandin, and J. No, Journal of Cosmology and Astroparticle Physics **2017**, 052–052 (2017).
[351] T. Kahniashvili, in *Workshop on Nonlinear Cosmology: Turbulence and Fields* (2005) arXiv:astro-ph/0508459.
[352] A. Roper Pol, S. Mandal, A. Brandenburg, T. Kahniashvili, and A. Kosowsky, Phys. Rev. D **102**, 083512 (2020), arXiv:1903.08585 [astro-ph.CO].
[353] D. J. Weir, Philosophical Transactions of the Royal Society A: Mathematical, Physical and Engineering Sciences **376**, 20170126 (2018).
[354] A. Kosowsky, A. Mack, and T. Kahniashvili, Physical Review D **66** (2002), 10.1103/physrevd.66.024030.
[355] Y. Akrami *et al.* (Planck), Astron. Astrophys. **641**, A9 (2020), arXiv:1905.05697 [astro-ph.CO].
[356] K. Martinovic, C. Badger, M. Sakellariadou, and V. Mandic, Phys. Rev. D **104**, L081101 (2021), arXiv:2103.06718 [gr-qc].
[357] K. Martinovic, P. M. Meyers, M. Sakellariadou, and N. Christensen, Phys. Rev. D **103**, 043023 (2021), arXiv:2011.05697 [gr-qc].
[358] H. Einsle, M.-A. Bizouard, T. Regimbau, and M. Sakellariadou, (2025), arXiv:2506.14764 [gr-qc].
[359] T. Regimbau, M. Evans, N. Christensen, E. Katsavounidis, B. Sathyaprakash, and S. Vitale, Phys. Rev. Lett. **118**, 151105 (2017), arXiv:1611.08943 [astro-ph.CO].
[360] S. Biscoveanu, C. Talbot, E. Thrane, and R. Smith, Phys. Rev. Lett. **125**, 241101 (2020), arXiv:2009.04418 [astro-ph.HE].
[361] S. Sachdev, T. Regimbau, and B. S. Sathyaprakash, Phys. Rev. D **102**, 024051 (2020), arXiv:2002.05365 [gr-qc].
[362] A. Sharma and J. Harms, Phys. Rev. D **102**, 063009 (2020), arXiv:2006.16116 [gr-qc].
[363] B. Zhou, L. Reali, E. Berti, M. Çalışkan, C. Creque-Sarbinowski, M. Kamionkowski, and B. S. Sathyaprakash, Phys. Rev. D **108**, 064040 (2023), arXiv:2209.01310 [gr-qc].
[364] M. Punturo *et al.*, Class. Quant. Grav. **27**, 194002 (2010).
[365] D. Reitze *et al.*, Bull. Am. Astron. Soc. **51**, 035 (2019), arXiv:1907.04833 [astro-ph.IM].